Quantum Metrology for Space-Based Tests of Gravitational Physics

Energy-Entangled photon pairs for probing general relativity with quantum states

Final Report

Authors: Prof. Andre Stefanov[1], Dr. Baenz Bassire[1], Dr. Jai Grover[2] , Mr. Alexander Hickey[2]
Affiliation: [1]University of Bern, [2]ESA ACT

Date: 28/02/2018

Contacts:

Andre Stefanov
Tel: +41 31 631 89 37
Fax: +41 31 631 37 65
e-mail: Andre.stefanov@iap.unibe.ch

Leopold Summerer (Technical Officer)
Tel: +31(0)715654192
Fax: +31(0)715658018
e-mail: act@esa.int

Available on the ACT website
http://www.esa.int/act

Ariadna ID: 17/1201
Ariadna study type: Standard
Contract Number: 4000000120842/17/NL/LF/as

Energy entangled photon pairs for probing general relativity with quantum states

Contents

I. Introduction

Systems that exploit the quantum properties of light and matter to achieve dramatic improvements in performance, are commonly referred to as quantum technologies (QT); these include, for example, quantum computing, sensing, metrology, imaging and communication. Recently, progress in quantum technologies has brought them out of the lab and onto the global stage, with major national and industrial actors expressing interest in their development and maturation. For example, in the European Union (EU) alone, we have the Quantum Technologies in Space (QTSpace) framework, funded as a Cooperation in Science and Technology (COST) action [1]. At an even larger scale is the EU funded billion Euro Quantum Technology flagship [2].

Quantum communication, in particular, is a field of growing importance. Here, the idea is to encode information in the quantum states of light, in such a way as to render communication robust against future

advancements in computing power (eg quantum computing), as well as secure against eavesdropping. Underlying most quantum communication protocols is the use of entangled photons [3, 4] for quantum key distribution (QKD) [5]. This makes use of the property of entangled systems that a measurement of the system necessarily perturbs the system, therefore eavesdroppers are easy to detect.

For the resulting quantum secure communication infrastructure to be global, the entangled photons need to be distributed over large distances [6]. In 2007 entangled photons were sent 144 km between European Space Agency (ESA) ground stations on two of the Canary Islands [7]. However, going further is a challenge because of the exponential photon loss with distance propagated through air or optical fibre - this places a limit of about 200km before photon loss is prohibitive [8].

Space provides an interesting framework for circumventing this limit, with entanglement being distributed through a satellite, or network of satellites in Earth orbit. Ideas along these lines have been pursued, for example, in the Quantum Entanglement for Space Experiments (space-QUEST) proposal, which hopes to demonstrate quantum communication from ground to the International Space Station (ISS) [9], as well as the Canadian Quantum Encryption and Science Satellite (QEYSSat) program [10].

However the first demonstration of entanglement distribution between ground and space was only recently performed by the Chinese MICIUS satellite in 2016 [11] as part of their Quantum Experiments at Space Scale (QUESS) mission. This development, while only a single demonstrator, has sparked a surge of interest in space based QKD, both in terms of maturing the technology requirements for a complete communications infrastructure, but also from the fundamental physics community looking to test basic principles of gravity and quantum mechanics.

The physical process of sending entangled photons over large distances through a gravitational potential is not fully understood based on current theory; this is because the behaviour of quantum systems in macroscopic regimes, of large mass or distance scale, has proven challenging to probe experimentally, and because there is no complete theory of quantum gravity as yet on which to base predictions.

Nevertheless there are various candidate theories, and some predict potentially observable effects on classical light: for instance a modified dispersion relation, which could be tested by interferometry [12, 13]; loss of coherence in single photon interferometry [14]; or even gravitationally induced decoherence of entangled photons [15].

As long as a complete theory of quantum gravity is not at hand, quantum field theory in curved space-time (QFTCS) [16] is the most accepted way to describe quantum systems in gravitational fields. In QFTCS, also known as semi-classical gravity, the gravitational field is modelled classically as a curved spacetime solution of General Relativity, while the other forces are modelled as quantum fields that propagate on this classical background. This serves as a useful proxy for a full theory, especially in regimes where the

curvature of spacetime is relatively small and gravitational effects correspondingly weak, as for example, in a near Earth environment.

In what follows we will use QFTCS as a reference against which to determine whether there exist effects due to the propagation of quantum states through a gravitational gradient. We will distinguish between those effects that are purely classical, those that arise from standard QFTCS, and finally those that are predicted by non-standard modifications beyond QFTCS.

Quantifying these effects is important from a fundamental perspective - when designing an experiment to test for them - but also from a practical one, when considering quantum key distribution. While classical gravitational effects could, in principle, be corrected for, decoherence effects would lead to an increased error rate. The error rate is a crucial parameter in QKD and sets the ultimate limits of a quantum communication channel. This situation, in which an effect is both a source of error to be characterised and a probe of fundamental physics, has also arisen in the context of satellite navigation systems, which are sensitive to gravitational time dilation effects.

Over the course of this document we describe various setups to measure an effect on quantum states, including entangled ones, when they are propagated through a gravitational potential. We first recall the expressions describing the propagation of light in a flat (section II) and curved (section III) spacetime. We then introduce the basic concepts of quantum field theory in section IV. We apply those concepts to the propagation of photon creation operators in section in flat and curved spacetime by making use of QFTCS (section V). Section VI contains the first main result of this study. We compute measurable quantities that are correlation functions of first order for single photon states or second order for photon pairs. We compare two approaches used in the literature but show that they lead to the same results. As we are specifically interested on the effects of general relativity on quantum states, we will look at three situations. The first one is the simplest case of a quantum state of light given by a single photon propagating from Alice to Bob (Fig. 1). However, a single photon doesn't show entanglement when detected by single photon detectors (homodyne detection could reveal single photon entanglement). Therefore we further investigate the simplest entangled states realized by photon pairs, detected either simply by coincidence (Fig. 2) or in an interferometric setup revealing their entanglement (Fig. 7) as in section VII. In evaluating the effects of gravity on quantum states, it is crucial to precisely define the measured quantities and the reference frames in which they are measured. Using standard QFTCS, we show that the relativistic effects on quantum states are fully equivalent to the ones on classical light and are therefore expected to be small in the vicinity of the Earth. Finally in section VIII we estimate the sensitivity of a quantum experiment between ground and space and evaluate the possibility of increasing the signal by making use of multiplexed single photon detectors.

II. Propagation of light in a flat spacetime

Before investigating the propagation of a photon on a Schwarzschild curved spacetime background we first consider the transfer function for a free-space propagation on a flat space metric. By doing so, we rely on the input-output relation of a classical electromagnetic (EM) field expressed by Fourier optics [17]. Let $E^+(\boldsymbol{\rho}_0, t_0)$ be the initial positive frequency part of the electric field provided by a classical light source at spacetime point $(\mathbf{r}_0, t_0)$ with $z_0 = 0$ and the transverse spatial coordinates given by $\boldsymbol{\rho}_0 = (\rho_{0x}, \rho_{0y})$. In general terms, a linear system may alter this field distribution according to

$$E^+(\mathbf{r}_1, t_1) = \int d^2\rho_0 \int dt_0 \; h(\mathbf{r}_1, \boldsymbol{\rho}_0, t_1, t_0) \; E^+(\boldsymbol{\rho}_0, t_0), \tag{1}$$

where $h(\mathbf{r}_1, \boldsymbol{\rho}_0, t_1, t_0)$ is denoted as the impulse-response function of the optical setup including the case of free-space propagation. A system is called time-invariant (shift-invariant) if a shift in time (space) of its input distribution leads to the same shift in time (space) of the output distribution without otherwise altering the shape of the latter. The impulse response-function can then be written as $h(\mathbf{r}_1, \boldsymbol{\rho}_0, t_1, t_0) = h(\boldsymbol{\rho}_1 - \boldsymbol{\rho}_0, z_1, t_1 - t_0)$ and, correspondingly, Eq. (1) reduces to a convolution. In the following we consider the system to be shift- and time-invariant. By inserting the Fourier decompositions of $E^+(\boldsymbol{\rho}_0, t_0)$ and the impulse-response function h, Eq. (1) can be expressed in Fourier space as

$$E^+(\mathbf{r}, t) = \int d^2q \int d\omega \; H(\boldsymbol{\rho}, z, \mathbf{q}, \omega) E^+(\mathbf{q}, \omega) e^{-i\omega t}, \tag{2}$$

where the function $H(\boldsymbol{\rho}, z, \mathbf{q}, \omega)$ is now denoted as transfer function and conveniently includes a plane wave phase, i.e. $H(\boldsymbol{\rho}, z, \mathbf{q}, \omega) = U(\mathbf{q}, \omega) \exp[i(\mathbf{q}\boldsymbol{\rho} + k_z z)]$. Here, $\mathbf{q} = (q_x, q_y)$ denotes the transverse coordinates of the momentum vector $\mathbf{k}$ [18].

III. Propagation of a light in a Schwarzschild spacetime

A. Spacetime geometry

The transfer function of Eq. (2) can now be generalised to describe the free radial propagation of light in a curved spacetime. We shall consider the spacetime surrounding a massive, non-spinning spherically symmetric body with mass M - a proxy for the Earth. The corresponding geometry is described in general

relativity by the $(3+1)$-Schwarzschild metric

$$-c^2 d\tau^2 = g_{\mu\nu} dx^\mu dx^\nu = -V(r)\, dt^2 + V^{-1}(r)\, dr^2 + r^2\, (d\theta^2 + \sin\theta^2 d\phi^2)\,, \tag{3}$$

where $V(r) = 1 - \frac{2M}{r}$, and we work in a signature $\{-,+,+,+,+\}$ [19]. Note that, where it is not indicated otherwise, we shall now use units in which $G = c = 1$. Here the metric is presented in the spherical-polar Schwarzschild coordinates $x^\mu = \{t, r, \theta, \varphi\}$, with r a circumferential radius - spheres will have circumference $2\pi r$ - and t the time as measured on the clock of an asymptotic, distant, observer that is stationary - moving only in time. These provide a global, outside the horizon, set of coordinates that are adapted to the symmetries of the solution; the Schwarzschild spacetime is the unique spherically symmetric, static, vacuum solution in general relativity [19].

In addition to the privileged asymptotic observer, one can also define local observers situated arbitrarily in the Schwarzschild spacetime - though outside the horizon - and moving on timelike (speed less than light) trajectories. These observers, in their own reference frame, measure a so-called proper time τ which corresponds to the path length along their spacetime trajectory $\tau = \int d\tau = \int \sqrt{-g_{\mu\nu} dx^\mu dx^\nu}$.

In particular, a static observer, with motion parallel to $T = \partial_t$, would find that along their trajectories $d\tau^2 = V(r) dt^2$; this follows from (3), where, since the observer is not moving in space, $dr = d\theta = d\phi = 0$. A straightforward integration then implies

$$\tau = \sqrt{V(r)}\, t\,. \tag{4}$$

Since $V(r \to \infty) = 1$ this is consistent with the notion that t is the proper time of the asymptotic observer. Note further that a timelike observer, who parametrises their trajectory by their proper time τ would find, from (3), that their velocity $U^\mu(x) = \frac{dx^\mu}{d\tau}$ sastisfies

$$U \cdot U = g_{\mu\nu} \frac{dx^\mu}{d\tau} \frac{dx^\nu}{d\tau} = -1\,. \tag{5}$$

To model the motion of light we shall work in the geometric optics approximation. In this limit light is taken to have a wavelength less than the curvature scale of the spacetime, and hence is ray-like and follows null geodesics. Geodesics are the straightest paths in a curved spacetime, corresponding to force-free motion under the influence of only gravity. The null condition further specifies that the geodesic motion is at the speed of light, which translates, in terms of the metric, into the requirement $ds^2 = 0$ along the trajectory; if $K(x)$ is the tangent vector to a null geodesic then $K \cdot K = 0$.

B. Gravitational redshift

Symmetries play a crucial role in determining the structure of a spacetime. Killing vectors are the generators of these symmetries eg rotations, or translations in time or space. The existence of a symmetry is formally specified by the vanishing of the Lie derivative of the metric with respect to a Killing vector. For example a static spacetime will have a Killing vector $T = \partial_t$ related to time translation invariance.

Associated to each of these Killing vectors is a conserved quantity. For instance the energy $E = -T \cdot K$ is conserved along geodesics for which $K(x)$ is the tangent vector. One can use this construction to determine the frequency shift of light sent between arbitrary observers in relative motion. The frequency of a light ray following a null geodesic with 4-momentum $K(x)$, detected by an observer with velocity $U_A(x)$ is given by $\omega_A = -K \cdot U_A$. Then

$$\frac{\omega_A}{\omega_B} = \frac{K \cdot U|_A}{K \cdot U|_B}. \tag{6}$$

In the particular case of static observers, whose velocity is proportional to the time translation Killing vector $U(x) = F(x)\, T$, we can say more. We use the fact that $T \cdot T = g(\partial_t, \partial_t) = g_{tt}$. Then, to satisfy $U \cdot U = -1$, we must have $F = 1/\sqrt{-g_{tt}}$.

We arrive at the following

$$\begin{aligned} \frac{\omega_A}{\omega_B} &= \frac{K \cdot U|_A}{K \cdot U|_B} \\ &= \frac{F_B}{F_A} \frac{K \cdot T|_A}{K \cdot T|_B} \\ &= \frac{F_B}{F_A} \\ &= N_{AB}\ , \end{aligned} \tag{7}$$

where we use the fact that the energy $E = -T \cdot K$ is a constant and introduced notation $N_{AB} = \frac{F_B}{F_A}$ that will prove useful later. For the Schwarzschild spacetime we find from (3) that $N_{AB} = \sqrt{\frac{V(r_B)}{V(r_A)}}$. Then, we can see from (7) that an asymptotic observer O at $r \to \infty$ will see a photon emitted at some radial position r and frequency ω as having a redshifted frequency

$$\omega_O = \sqrt{V(r)}\, \omega = \sqrt{1 - \frac{2M}{r}}\, \omega\ . \tag{8}$$

C. A two dimensional model

Since we are mostly interested in the description of radially propagating light, travelling from its source located at the surface of the Earth to a receiver on a satellite, we shall restrict our attention to the $(1 + 1)$

form (i.e. with no angular dependence) of Eq. (3) given by

$$ds^2 = -V(r)\, dt^2 + V^{-1}(r)\, dr^2 \,. \tag{9}$$

We can further simplify this form of the metric by using the fact that any two dimensional spacetime is conformally flat [19]. This becomes manifest by rewriting Eq. (9) using the tortoise coordinate

$$x = x(r) = r + 2M \log\left(\frac{r}{2M} - 1\right) \,, \tag{10}$$

so that

$$ds^2 = V(r)(-dt^2 + dx^2) \,. \tag{11}$$

Note that the coordinate x is only defined outside the horizon $r > 2M$ and that it satisfies $dx = V(r)^{-1}\, dr$. In these coordinates the propagation of light rays, for which $ds^2 = 0$, matches that of flat space with

$$\frac{dx}{dt} = \pm 1 \tag{12}$$

IV. Quantum field theory

()

We want to describe the propagation of quanta of light, photons, between radially distributed observers in a gravitational field. So far we have arrived a description of *classical* light rays propagating through a curved spacetime (or, equivalently, gravitational field). A proper description of *quantised* light requires a formulation in terms of quantum field theory (QFT). In this section we briefly review the salient parts of the the QFT framework that we will need. For simplicity, and without too much loss of generality, we will work with a scalar field as a simple proxy for an EM field.

In particular we look at Klein-Gordon (KG) theory for a massive real scalar field ϕ, with action

$$I = \int (-\frac{1}{2} g^{ab} \partial_a \phi \partial_b \phi - \frac{1}{2} m^2 \phi^2) \sqrt{-g}\, d^4x \,, \tag{13}$$

and equations of motion

$$g^{ab} \nabla_a \nabla_b \phi - m^2 \phi = 0 \,. \tag{14}$$

Here g_{ab} represents the spacetime metric tensor with $a, b = (t, \mathbf{x})$, and g^{ab} the metric inverse.

The canonical momentum conjugate to ϕ is obtained by varying the action

$$\Pi(x) = \frac{\delta I}{\delta(\partial_t \phi(x))} = \sqrt{-g} g^{ta} \partial_a \phi(x) \tag{15}$$

Now, the general procedure for quantization is to promote ϕ and Π to operators, and impose the canonical commutation relations (units: $\hbar = 1$)

$$[\phi(t,x), \Pi(t,x')] = i\delta^{(3)}(x-x'), \quad [\phi(t,x), \phi(t,x')] = 0$$
$$[\Pi(t,x), \Pi(t,x')] = 0\ . \tag{16}$$

What we lack, and will now attempt to introduce, is a Hilbert space of states that these operators act on. Let $\mathcal{S}$ be the space of complex solutions of the KG equation.

A. Quantum field theory in a flat spacetime

First consider the case that the metric is flat, $g_{ab} = \eta_{ab} = \text{diag}(-1,1,1,1)$. We begin by defining an inner product on $\mathcal{S}$. This is the KG inner product

$$(\phi_1, \phi_2) = -i\int_{\Sigma_t} (\phi_1 \partial_t \bar{\phi}_2 - \phi_2 \partial_t \bar{\phi}_1) d^3\mathbf{x}\ , \tag{17}$$

for $\phi_1, \phi_2 \in \mathcal{S}$. This inner product has some important properties: it is independent of the constant time surface Σ_t over which it is defined, a consequence of Stoke's theorem and the KG equation; moreover $(\phi_1, \phi_2) = \overline{(\phi_2, \phi_1)}$ so that it is Hermitian. However note that

$$(\phi_1, \phi_2) = -(\bar{\phi}_2, \bar{\phi}_1)\ , \tag{18}$$

so that $(\phi, \phi) = -(\bar{\phi}, \bar{\phi})$. This means that the inner product $(,)$ is not positive definite. Note also that $(\phi, \bar{\phi}) = -(\phi, \bar{\phi}) = 0$.

The elementary solutions to the KG equations of motion take the form of plane waves

$$\phi(x) = \phi_0 e^{ik_a x^a} = \phi_0 e^{-i\omega t + i\mathbf{k}\cdot\mathbf{x}}\ , \tag{19}$$

where $k^a = (\omega, \mathbf{k})$ and the frequency ω must satisfy the condition $k^2 = -\omega^2 + \mathbf{k}^2 = -m^2$. This implies that for any given spatial vector $\mathbf{k}$ there is a solution ω that is determined up to a sign.

In particular, the inner product is positive definite on $\mathcal{S}_k$ of positive frequency solutions to the KG equation

$$f_{\mathbf{k}}(x) = \frac{1}{(2\pi)^3 2\omega} e^{ik_a x^a}, \quad \omega = \sqrt{\mathbf{k}^2 + m^2}\ . \tag{20}$$

By positive frequency we mean that the time derivative pulls down a factor of $-i\omega$ with $\omega > 0$. That is

$$\partial_t f_{\mathbf{k}} = -i\omega f_{\mathbf{k}}, \quad \omega > 0\ . \tag{21}$$

One can also arrive at negative frequency modes by taking the complex conjugate of $f_{\mathbf{k}}$

$$\partial_t \bar{f}_{\mathbf{k}} = i\omega \bar{f}_{\mathbf{k}}, \quad \omega > 0\ . \tag{22}$$

These are orthogonal to the positive frequency plane waves, as mentioned earlier, and so we have the orthogonal decomposition $\mathcal{S} = \mathcal{S}_{\mathbf{k}} \oplus \bar{\mathcal{S}}_{\mathbf{k}}$ where $(,)$ is negative definite on $\bar{\mathcal{S}}_{\mathbf{k}}$.
Putting this all together, a general expression for the quantum operator $\phi(x)$ is

$$\phi(x) = \int (a_{\mathbf{k}} f_{\mathbf{k}}(x) + a^{\dagger}_{\mathbf{k}} \bar{f}_{\mathbf{k}}(x)) d^3\mathbf{k} \, , \tag{23}$$

where the $a_{\mathbf{k}}$ ($a^{\dagger}_{\mathbf{k}}$) are the coefficients of the positive (negative) frequency modes in the expansion:

$$a_{\mathbf{k}} = (f, \phi), \quad a^{\dagger}_{\mathbf{k}} = -(\bar{f}, \phi) \, . \tag{24}$$

They have the familiar interpretation of creation and annihilation operators, satisfying

$$\begin{aligned} &[a_{\mathbf{k}}, a^{\dagger}_{\mathbf{k}'}] = i\delta^{(3)}(\mathbf{k} - \mathbf{k}'), \quad [a_{\mathbf{k}}, a_{\mathbf{k}'}] = 0 \\ &[a^{\dagger}_{\mathbf{k}}, a^{\dagger}_{\mathbf{k}'}] = 0 \, , \end{aligned} \tag{25}$$

and we can construct N-particle states in the usual way, by successive application of creation operators on a ground state $|0\rangle$ defined so that $a_{\mathbf{k}}|0\rangle = 0, \forall k$.

B. Quantum field theory in a curved spacetime

For curved spacetimes we could follow the exact same scheme - with some small variations to accommodate the non-trivial metric. The problem we face is that there is no unique definition of "positive frequency" unless the spacetime is stationary. Hence there is no preferred way to decompose $\mathcal{S}$ as above. Instead, we simply choose a subspace $\mathcal{S}_{\mathbf{k}}$ for which $(,)$ is positive definite. In general there will be many ways to do this, for example corresponding to different observers/detectors who will use the proper time τ they measure along their trajectory to setup the decomposition.
Suppose we work with a complete set of orthonormal modes $f(x)$ with properties as above, and defined with respect to a more general KG inner product

$$(\phi_1, \phi_2) = \int_{\Sigma} n^a j_a \sqrt{\gamma} d^3\mathbf{x} \, , \tag{26}$$

where the KG current $j = -i(\phi_1 d\bar{\phi}_2 - \phi_2 d\bar{\phi}_1)$ and n_a is the normal to the space-like hypersurface Σ; in the case that this is a constant time surface as in the previous flat space definition then $n = dt$. We can proceed as before to perform a mode decomposition in terms of negative and positive frequency modes and their associated coefficients - interpreted again as creation and annihilation operators respectively

$$a(f) = (f, \phi), \quad a^{\dagger}(f) = -(\bar{f}, \phi) \, . \tag{27}$$

One can then define a ground state

$$a(f)|0\rangle_f = 0, \quad \forall f \in \mathcal{S}_{\mathbf{k}} \,, \tag{28}$$

and given some basis $\{f_i\}$ of $\mathcal{S}_{\mathbf{k}}$ the N-particle states $a^\dagger_{i_1}...a^\dagger_{i_N}|0\rangle_f$. We then choose the Hilbert space to be the Fock space spanned by the vacuum state, the 1-particle states, the 2-particles states etc.

In a general curved spacetime there is no preferred choice of $\mathcal{S}_{\mathbf{k}}$, instead there will be many inequivalent choices. Let $\tilde{\mathcal{S}}_{\mathbf{k}}$ be another choice of positive frequency subspace. Then any modes $g(x) \in \tilde{\mathcal{S}}_{\mathbf{k}}$ can be decomposed uniquely as $g = f + \bar{f}'$ with $f, f' \in \mathcal{S}_{\mathbf{k}}$. Hence

$$a(g) = (f + \bar{f}', \phi) = a(f) - a^\dagger(f') \,, \tag{29}$$

so that $a(f')|0\rangle_f \neq 0$ and $|0\rangle_f$ is no longer the vacuum state if one uses $\tilde{\mathcal{S}}_{\mathbf{k}}$ as the positive frequency subspace. Since the vacuum state depends on the choice of $\mathcal{S}_{\mathbf{k}}$, so does the definition of 1-particle states etc. So there is no natural notion of particles in a general curved spacetime.

Why doesn't this happen in the flat background? Consider a boost into a new frame with $t' = \gamma(t - \mathbf{v}\cdot\mathbf{x}), \quad \mathbf{x}' = \gamma(\mathbf{x} - \mathbf{v}t)$. Then the time derivative of the mode functions, say $f_{\mathbf{k}(x)}$ is

$$\begin{aligned} \partial_{t'} f_{\mathbf{k}} &= \frac{\partial x^a}{\partial t'} \partial_a \mathbf{k} \\ &= \gamma(-i\omega + i\mathbf{v}\cdot\mathbf{k})\mathbf{k} \\ &= -i\omega'\mathbf{k} \,. \end{aligned} \tag{30}$$

where ω' is the frequency in the transformed frame. This tells us that the modes are transformed into each other, with boosted momenta, and thus, crucially, the particle number operator and the vacuum state are invariant.

In a stationary (equilibrium) spacetime, one can use the time translation symmetry to identify a preferred choice of $\mathcal{S}_{\mathbf{k}}$. In particular there will exist a Killing vector field $T = \partial_t$ which generates a flow along which the metric is invariant

$$\mathcal{L}_T g_{ab} = 0 \,. \tag{31}$$

It is natural to use T to define the decomposition into negative/positive modes. This will coincide with the behaviour of a detector whose trajectory follows the orbit of the Killing field - such as a static observer moving only in time. We will make use of such observers in what follows when considering photon propagation in the Schwarzchild spacetime.

V. Propagation of a photon

A. Propagation of a photon in a flat spacetime

That quantum field operators transform in the same manner as classical fields is justified in [20]. We therefore write the photon operator which propagates a photon with frequency ω and transverse momentum $\mathbf{q}$ from $z_0 = 0$, through an optical setup (or solely free space) to a spacetime point $(\mathbf{r}, t)$ according to

$$a(\mathbf{r}, t) = a(\boldsymbol{\rho}, z, t) = \int d^2q \int d\omega \; H(\boldsymbol{\rho}, z, \mathbf{q}, \omega) a_{\mathbf{q},\omega} \mathrm{e}^{-i\omega t}. \tag{32}$$

Note, that for convenience we write operators without hat throughout this document. This photon operator annihilates a photon at $(\mathbf{r}, t)$ where the corresponding creation operator is given by $a^\dagger(\mathbf{r}, t) = [a(\mathbf{r}, t)]^\dagger$. The photon operators obey

$$\left[a(\mathbf{r}, t), a^\dagger(\mathbf{r}', t')\right] = \int d^2q \int d\omega \; H(\boldsymbol{\rho}, z, \mathbf{q}, \omega) H^*(\boldsymbol{\rho}', z', \mathbf{q}, \omega) \mathrm{e}^{i\omega(t'-t)} \tag{33}$$

and all other commutators being zero.

The free-space propagation of a photon in flat space geometry and in paraxial approximation, i.e. its wave vector makes only a small angle to the optical axis, is given by

$$H(\boldsymbol{\rho}, z, \mathbf{q}, \omega) = \mathrm{e}^{i\left(k(\omega)z - \frac{|\mathbf{q}|^2 z}{2k(\omega)}\right)} \mathrm{e}^{i\mathbf{q}\boldsymbol{\rho}} \tag{34}$$

and $k(\omega) = \omega/c \, n(\omega)$ is the corresponding dispersion relation with $n(\omega) = 1$ for free-space propagation. In the following we consider only propagation modes according to a plane wave and thus Eq. (34) is reduced to

$$H(z, \omega) = \mathrm{e}^{ik(\omega)z}. \tag{35}$$

The corresponding operator then reads

$$a(z, t) = \int_0^\infty d\omega \mathrm{e}^{ik(\omega)z} a_\omega \mathrm{e}^{-i\omega t}. \tag{36}$$

Here, we explicitly indicate the integration boundaries to emphasize that absolute frequencies are considered.

B. Propagation of a photon in a Schwarzschild spacetime

When considering wavepackets in a curved spacetime we need to be mindful of the ambiguity mentioned in Section IV B; in general different observers, in various states of motion through spacetime, will each have their own notion of local proper time. This suggests that we should attempt to define our wavepacket creation operators in a local region, with compact support, and with respect to the proper time of the observer/detector performing the experiment. This approach was adopted in the series of papers beginning with [21–23].

There is, however, an alternative picture that can be considered. Here we uses the fact that the Schwarzschild spacetime has a preferred time coordinate, t associated to the time translation Killing vector $T = \partial_t$. With this coordinate and the conformal radial coordinate we can adopt a formalism using global Schwarzschild coordinates that closely resembles that of the flat space photon propagation transfer functions. This approach was adopted in the series of papers starting with [15] that propose an 'event operator' formalism.

In what follows we will, at least initially, adopt both formalisms and highlight their features; however, in a bit of foreshadowing, let us say that in a stationary spacetime like Schwarzschild these methods are essentially equivalent and one can pass between them without complication.

1. Creating localised wavepackets

A wavepacket localised in space is defined through a $\mathbb{C}$-valued distribution $F_{x_0}(x)$ centred on a position x_0. Corresponding annihilation operators take the form

$$\begin{aligned} a_{x_0}(t) &= \int_0^\infty dx F_{x_0}(x) a(t,x) \\ &= \int_0^\infty dx F_{x_0}(x) \big(\int_0^\infty d\omega e^{i\omega(x-t)} a_\omega \big) \\ &= \int_0^\infty d\omega F_{\omega_0}(\omega) e^{-i\omega t} a_\omega \ . \end{aligned} \tag{37}$$

The last expression coincides with the definition of the wave packet annihilation operator in [21] where we write

$$a_{\omega_0}(t) = \int_0^\infty d\omega F_{\omega_0}(\omega) e^{-i\omega t} a_\omega \ . \tag{38}$$

Based on (37), the operator describing the creation and annihilation of a photon wavepacket can be expressed in any frame as

$$a_{\Omega_{K0}}(\tau_K) = \int_0^\infty d\Omega_K e^{-i\Omega_K \tau_K} F^K_{\Omega_{K0}}(\Omega_K) a_{\Omega_K} \ , \tag{39}$$

where $K = A, B, O$. The Ω_K are the proper frequencies of the observers corresponding to proper time τ_K as measured in their labs. The $F^K_{\Omega_{K0}}$ are frequency distributions (Fourier transforms of the spatial distribution as per the last section) of the wavepacket centred on Ω_{K0}. The asymptotic observer on a static spacetime has a privileged role but fits within the same formalism.

We can relate the mode operators and the frequency distributions of static observers, say Alice A and Bob B, located at different radial positions in the spacetime. To do this we use first the canonical commutation relations in each frame

$$[a_{\Omega_K}, a^\dagger_{\Omega'_K}] = \delta(\Omega_K - \Omega'_K) \,, \tag{40}$$

as well as the relation (7) between the frequencies observed in each frame $\Omega_A = N_{AB}\,\Omega_B$ where

$$N_{AB} = \sqrt{V(r_B)/V(r_A)} = 1/N_{BA} \,. \tag{41}$$

Note that this and the following expressions should be understood generally, for whatever choice of A, B we use; for example we could set 'B' to be the asymptotic observer in which case $N_{AO} = \sqrt{1/V(r_A)}$ as in (8). Then, using a standard property of delta functions, we find that

$$\delta(\Omega_A - \Omega'_A) = \frac{\delta(\Omega_B - \Omega'_B)}{N_{AB}} \,. \tag{42}$$

If we substitute this in the commutation relations we get

$$[a_{\Omega_A}, a^\dagger_{\Omega'_A}] = \frac{1}{N_{AB}} [a_{\Omega_B}, a^\dagger_{\Omega'_B}] \,, \tag{43}$$

so that

$$a_{\Omega_A} = \frac{1}{\sqrt{N_{AB}}}\, a_{\Omega_B} \,. \tag{44}$$

Next, noting that the product $\Omega_K \tau_K$ is an invariant we can rewrite (39) as

$$\begin{aligned} a_{\Omega_{A0}}(\tau_A) &= \int_0^\infty (N_{AB}\, d\Omega_B)\, e^{-i\Omega_B \tau_B} F^A_{\Omega_{A0}}(\Omega_A) \frac{a_{\Omega_B}}{\sqrt{N_{AB}}} \\ &= \int_0^\infty d\Omega_B\, e^{-i\Omega_B \tau_B} (\sqrt{N_{AB}}\, F^A_{\Omega_{A0}}(N_{AB}\,\Omega_B))\, a_{\Omega_B} \,. \end{aligned} \tag{45}$$

Since the $a_{\Omega_{K0}}(\tau_K)$ are supposed to describe the same photon wave packet, just in different frames, we can conclude that the frequency distributions are related by

$$F^B_{\Omega_{B0}}(\Omega_B) = \sqrt{N_{AB}} F^A_{\Omega_{A0}}(N_{AB}\,\Omega_B) \,. \tag{46}$$

This means that the local wavepacket measured by Bob will be a modified version of the wavepacket initially sent by Alice. If a measurement process - eg communication or key distribution - works on the basis of only local protocols, then there will be in principal a mismatch between Bob's expectations and what he receives; this could be interpreted as a noisy channel [21] (see Section VI B).

This formalism, on the other hand, has less in common with the flat space formalism; in particular the wavepackets so defined are not propagating.

2. *Creating propagating wavepackets*

By considering the plane wave solution modes from the Klein-Gordon equation [21] in a conformally flat metric we can identify the free-space propagating photon field operator in curved spacetime to be

$$a_{\omega_0}(x,t) = \int_0^\infty d\omega F_{\omega_0}(\omega) \mathrm{e}^{i\omega(x-t)} a_\omega \tag{47}$$

with x given by Eq. (10) and $k(\omega) = \omega$. Under the perspective of Eq. (47) being a creation operator, the additional function $F_{\omega_0}(\omega)$ is the spectral distribution function centred around ω_0 of the photon created at spacetime point (x,t). Being an annihilation operator, $F_{\omega_0}(\omega)$ describes the spectral response of the photon annihilation device, i.e. the detector. The corresponding commutator is given by

$$\left[a_{\omega_0}(x,t), a^\dagger_{\omega_0}(x',t')\right] = \int_0^\infty d\omega \ |F_{\omega_0}(\omega)|^2 \ \mathrm{e}^{i\omega[(x-x')-(t-t')]} \ , \tag{48}$$

where we used that $\left[a_\omega, a^\dagger_{\omega'}\right] = \delta(\omega - \omega')$. In particular, we obtain for $x = x'$ and $t = t'$

$$\left[a_{\omega_0}(x,t), a^\dagger_{\omega_0}(x,t)\right] = 1 \ , \tag{49}$$

under the condition that the wavepacket is normalised

$$\int_0^\infty d\omega |F_{\omega_0}(\omega)|^2 = 1 \ . \tag{50}$$

For an infinite bandwidth, i.e. $F_{\omega_0}(\omega) = 1$, we obtain

$$\left[a_{\omega_0}(x,t), a^\dagger_{\omega_0}(x',t')\right] = \delta(\Delta x - \Delta t), \qquad \Delta x = x - x', \qquad \Delta t = t - t' \ , \tag{51}$$

i.e. the commutator is non-vanishing on the null separated world-line. Equations (49) and (51) imply that the operators do not commute along null world lines. For spacelike or timelike separations the commutator is a decaying function of the separation.

One can also see that the operators (47) have support along the entire geodesic [15], since $a(x,t) = a(x + d, t + d)$. Moreover, notice that the operator of Eq. (47) incorporates an explicit radial position dependence

x in the phase. These are both in contrast to the local definition used in Equations (38) and (37) and the work of [21].

In the spirit of Eq. (35), the transfer function for a free-space propagation in a Schwarzschild metric is then identified as

$$H(x_k,\omega) = \mathrm{e}^{i\omega x_k} = \mathrm{e}^{i\omega\left[r_k + 2M\log\left(\frac{r_k}{2M}-1\right)\right]}\,, \tag{52}$$

where instead of the longitudinal coordinate z_k we invoke x_k for a radial distance. From now on, the index k will refer to the radial position of a specific observer k in the coordinate system of the asymptotic observer.

VI. Correlation functions

In the following we describe various experimental situations on the curved spacetime background introduced in Section V B. We restrict our calculations to the fundamental cases of one photon and entangled photon pairs. We are interested in estimating the relevant observable related to photon counting which are the first-order correlation function (single photon counting) for the case of one photon states and second-order correlation function (2 fold coincidence counting) for photon pairs [24]. Thereby, we formulate the results on the one hand in the local shell coordinates introduced in Section V B 1 and on the other hand in the reference frame of the asymptotic observer discussed in Section V B.

A. First-order correlation function: Experimental scenario

In a first experimental setting we consider the scenario where Alice and Bob are situated at two different heights in a gravitational potential. Alice resides in her laboratory on the surface of the earth at radial coordinate $r_A = r_E$ and Bob is on on a satellite with constant radius $r_B = r_E + h$ and having no angular motion with respect to Alice (Fig.1). Alice sends a photon described by a wavepacket to Bob which annihilates it via a point-like single photon detector. The detection of a single photon is formally described by a first-order correlation function [24] which represents the probability per unit time that a photon is registered by the detector.

B. First-order correlation function in local coordinates

We first consider the scenario shown by Fig. 1 in the local coordinates of Alice and Bob. This framework relies upon the formalism presented in [21] revised in V B 1.

Alice prepares a photon wavepacket in her laboratory with respect to her clock providing the proper time

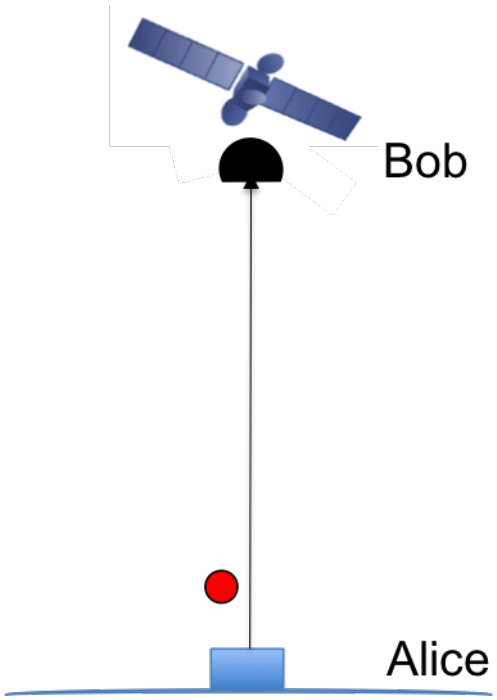

FIG. 1. A photon is emitted at Alice and detected by Bob.

τ_A. The corresponding photon operator reads

$$a_{\Omega_{A0}}(\tau_A) = \int_0^\infty d\Omega_A e^{-i\Omega_A\tau_A}\bar{\Lambda}^A_{\Omega_{A0}}(\Omega_A)a_{\Omega_A}\ , \tag{53}$$

and includes a frequency distribution of the wavepacket centered around the peak frequency Ω_{A0}. ($\bar{\Lambda}$ denotes the complex conjugate of Λ.) The corresponding single photon state generated at the initial central time $\tau_{Ai} = 0$ in the lab of Alice is then given by

$$|\Psi_1\rangle = \int_0^\infty d\Omega_A \Lambda^A_{\Omega_{A0}}(\Omega_A)a^\dagger_{\Omega_A}|0\rangle. \tag{54}$$

Bob detects the photon in his laboratory using his clock with its proper time τ_B at the final time τ_{Bf}.His detector annihilates a photon described by the operator

$$a_{\Omega_{B0}}(\tau_{Bf}) = \int_0^\infty d\Omega_B e^{-i\Omega_B\tau_{Bf}}F^B_{\Omega_{B0}}(\Omega_B)a_{\Omega_B}\ , \tag{55}$$

with a spectral response function $F^B_{\Omega_{B0}}(\Omega)$. The corresponding single photon projection operator reads

$$\Pi^{(1)}(\tau_{Bf}) = a^\dagger_{\Omega_{B0}}(\tau_{Bf})|0\rangle\langle 0|a_{\Omega_{B0}}(\tau_{Bf})\ , \tag{56}$$

and with this the first-order correlation function is given by

$$\begin{aligned} G^{(1)}(\tau_{Bf}) &= \langle\Psi_1|\Pi^{(1)}(\tau_{Bf})|\Psi_1\rangle \\ &= \langle 0|a_{\Omega_{A0}}(0)a^\dagger_{\Omega_{B0}}(\tau_{Bf})|0\rangle\langle 0|a_{\Omega_{B0}}(\tau_{Bf})a^\dagger_{\Omega_{A0}}(0)|0\rangle \\ &= |\psi_1(\tau_{Bf})|^2. \end{aligned} \tag{57}$$

The single-photon wavefunction expressed in the local frame of Bob reads

$$\begin{aligned}
&\psi_1(\tau_{Bf}) = \langle 0|a_{\Omega_{B0}}(\tau_{Bf})a^\dagger_{\Omega_{A0}}(0)|0\rangle \\
&= \int_0^\infty d\Omega_B d\Omega_{A1}\Lambda^A_{\Omega_{A0}}(\Omega_{A1})F^B_{\Omega_{B0}}(\Omega_B)[a_{\Omega_B}, a^\dagger_{\Omega_{A1}}]e^{-i\Omega_B\tau_{Bf}} \\
&= \int_0^\infty d\Omega_B d\Omega_{B1}\sqrt{N_{AB}}\Lambda^A_{\Omega_{A0}}(N_{AB}\Omega_{B1})F^B_{\Omega_{B0}}(\Omega_B)\delta(\Omega_B-\Omega_{B1})e^{-i\Omega_B\tau_{Bf}} \\
&= \int_0^\infty d\Omega_B \sqrt{N_{AB}}\Lambda^A_{\Omega_{A0}}(N_{AB}\Omega_B)F^B_{\Omega_{B0}}(\Omega_B)e^{-i\Omega_B\tau_{Bf}} \\
&= \int_0^\infty d\Omega_B \Lambda^B_{\Omega_{B0}}(\Omega_B)F^B_{\Omega_{B0}}(\Omega_B)e^{-i\Omega_B\tau_{Bf}}\ ,
\end{aligned} \tag{58}$$

where we used the relation of Eq. (44) and the gravitational redshift formula $\Omega_A = N_{AB}\Omega_B$. The first-order correlation function is therefore given by the product of the spectrum $\Lambda^B_{\Omega_{B0}}(\Omega)$ measured in Bob's local frame and the response function of its detector.

1. Fidelity

The wavepacket $\Lambda^B_{\Omega_{B0}}(\Omega)$ as measured by Bob is different, in its shape and central frequency, from the wavepacket $\Lambda^A_{\Omega_{A0}}(\Omega)$ originally generated by Alice. The particular relation between the two frequency distributions is given by Eq. (46) and is specific to the Schwarzschild metric. A possible quantification for the deviation between the two measured wavepackets is given by their fidelity - this is can then be considered as a measure of the quality of the communication channel between the two observers [21]. In quantum mechanics the fidelity F is formally defined as the overlap between two states, say $|\psi\rangle$ and $|\psi'\rangle$, such that $F = |\langle\psi'|\psi\rangle|^2 = |\Delta|^2$ and $\Delta \doteq \langle\psi'|\psi\rangle$. It can be realized by measuring one of the states with a detector defined by the other state. If we intend to use F as a measure of the quality of a transmission channel, as done in [21], we have to first agree on the relationship between the Hilbert space at each end of the channel. For example, when polarized light is transmitted from Alice to Bob, they have to agree in advance on the relative orientation of their measurement devices. Similarly, if time and frequency are the quantities of interest, they have to agree on their definition of time. In a flat spacetime this is trivially done by using identical clocks. In curved space-time the value of the fidelity for the channel will depend on how Alice and Bob clocks (or frequency references) are synchronized.

To calculate the fidelity we take into account Eq. (54) and define this state as $|\Psi^A_1\rangle \doteq |\Psi_1\rangle$. Accordingly, we introduce

$$|\Psi^B_1\rangle = \int_0^\infty d\Omega_B \Lambda^B_{\Omega_{B0}}(\Omega_B)a^\dagger_{\Omega_B}|0\rangle\ , \tag{59}$$

where Λ^B_Ω now determines the spectrum measured by Bob. The fidelity Δ^B evaluated in the local frame of Bob is then calculated to be

$$\begin{aligned}\Delta^B &= \langle 0|a_{\Omega_{B0}}(0)a^\dagger_{\Omega_{A0}}(0)|0\rangle \\ &= \int_0^\infty d\Omega_A d\Omega_B \Lambda^A_{\Omega_{A0}}(\Omega_A)\bar{\Lambda}^B_{\Omega_{B0}}(\Omega_B)[a_{\Omega_B}, a^\dagger_{\Omega_A}] \\ &= \int_0^\infty d\Omega_B \sqrt{N_{AB}}\Lambda^A_{\Omega_{A0}}(N_{AB}\Omega_B)\bar{\Lambda}^B_{\Omega_{B0}}(\Omega_B) \\ &= \int_0^\infty d\Omega_B |\Lambda^B_{\Omega_{B0}}(\Omega_B)|^2 \\ &= 1\,, \end{aligned} \tag{60}$$

if we assume the spectrum to be normalized. We further used Eq. (44) and Eq. (46). Equation (60) takes into account the transformation of the wavepacket sent by Alice due to the redshift accumulated during its propagation to Bob. In other words it assumes some knowledge on Bob's part, about the initial properties of the wavepacket as measured by Alice, such that he can perform the correct redshift transformation and corresponding projection distribution, to obtain $F = 1$. Note that the additional linear spectral phase corresponding to the time delay of the photon propagating from Alice to Bob, and incorporating the curvature of space, has not been considered in the above calculation. This is because the additional phase does not play a role for measurements in the spectral domain and, in the time domain, a linear phase leads to a time shift which can be compensated for through the timing of the detector. Equation (60), however, seems to contradict [21] in which the fidelity of the channel is expressed in terms of

$$\Delta = \int_0^\infty d\Omega \bar{\Lambda}^B_{\Omega_{B0}}(\Omega)\Lambda^A_{\Omega_{A0}}(\Omega)\,. \tag{61}$$

With this definition we calculate the Fidelity F to be $F = |\Delta|^2 \sim 1 - 5 \times 10^{-11}$ for Earth-to-LEO (low Earth orbit) communication with $h = 500\,\text{km}$ and a Gaussian spectrum with a width of $\Delta\lambda = 100\,\text{nm}$. The difference in this approach to the fidelity calculation lies in the tacit assumption that Alice and Bob are using identical clocks and operating as though they were both in flat space ie not taking any relativistic effects (red shift) into account. The fidelity is then the overlap between the state received by Bob, $\bar{\Lambda}^B_{\Omega_{B0}}(\Omega)$, and the state measured by Bob - he projects onto an undistorted version of the state Alice prepared assuming a flat space propagation - $\bar{\Lambda}^A_{\Omega_{A0}}(\Omega)$.

Note that Eq. (61) can be expressed in the Fourier domain as

$$\Delta = \int_0^\infty d\tau\, \bar{\psi}^B_1(\tau)\psi^A_1(\tau)\,, \tag{62}$$

with $\psi^B_1(\tau)$ given by Eq. (58) and $\psi^A_1(\tau)$ accordingly. In order to measure the fidelity defined in Eq. (61) or the equivalent expression in the time domain Eq. (62), one would need to experimentally realize a projection

onto well defined states. However, projective measurements in the energy or temporal domain are usually only done onto restricted set of states (e.g. the frequency bins of a spectrometer). As a consequence, Bob would need to perform a complete quantum state reconstruction to evaluate Eq. (61) or Eq. (62).

C. First-order correlation function in Schwarzschild coordinates

We now consider the scenario of Fig. (1) in the coordinate system of the asymptotic observer with radial coordinate $r \to \infty$. This observer has its proper time coordinate t which is equal to the time coordinate appearing in the Schwarzschild metric. In the case of the asymptotic view, there is only one observer, i.e. one clock, involved in the description of the process. In this formalism we will explicitly include the radial position coordinate $x_k = x_k(r_k)$ in the phase factor of the photon operator. This allows us to represent the propagation of a photon along the radial direction in the Schwarzschild metric via the free-space transfer function of Eq. (52). We consider again the scenario where Alice resides on the surface of the Earth, i.e. $x_A = x_A(r_E)$, and Bob is on a satellite at a radial distance $x_B = x_B(r_E + h) > x_A$ from the center of the Earth; note, the radius of the Earth is much larger than the Schwarzschild radius $r_S/r_E \sim 1.4 \times 10^{-9}$. A photon wavepacket with central frequency ω_0 is generated in Alice's lab at radial position x_A and initial time t_i. The corresponding photon operator reads

$$a_{\omega_0}(x_A, t_i) = \int_0^\infty d\omega \bar{\Lambda}_{\omega_0}(\omega) \mathrm{e}^{i\omega(x_A - t_i)} a_\omega \ . \tag{63}$$

In contrast to the local formalism, we do not apply a further label to $F_{\omega_0}(\omega)$ since we only consider a single spectral distribution in the global frame of the asymptotic observer. This distribution remains unaltered during the propagation of the photon. The one-photon state at $t_i = 0$ reads

$$|\Psi_1\rangle = \int_0^\infty d\omega \Lambda_{\omega_0}(\omega) \mathrm{e}^{-i\omega x_A} a_\omega^\dagger |0\rangle \ . \tag{64}$$

The photon operator at the radial position of Bob and the final time t_f of the detection is

$$a_{\omega_0}(x_B, t_f) = \int_0^\infty d\omega F_{\omega_0}(\omega) \mathrm{e}^{i\omega(x_B - t_f)} a_\omega \ , \tag{65}$$

with $F_{\omega_0}(\omega)$ describing the spectral response of the detector. Using the corresponding projection operator of Eq. (56) we obtain for the first-order correlation function

$$\begin{aligned} G^{(1)}(x_A; x_B, t_f) &= \langle \Psi_1 | \Pi^{(1)}(x_B, t_f) | \Psi_1 \rangle \\ &= \langle 0 | a_{\omega_0}(x_A, 0) a_{\omega_0}^\dagger(x_B, t_f) | 0 \rangle \langle 0 | a_{\omega_0}(x_B, t_f) a_{\omega_0}^\dagger(x_A, 0) | 0 \rangle \\ &= |\psi_1(x_A; x_B, t_f)|^2 \ , \end{aligned} \tag{66}$$

with the one-photon wavefunction

$$\begin{aligned}\psi_1(x_A;x_B,t_f) &= \langle 0|a_{\omega_0}(x_B,t_f)a^\dagger_{\omega_0}(x_A,0)|0\rangle \\ &= \int_0^\infty d\omega_1 d\omega_2 F_{\omega_0}(\omega_1)\Lambda_{\omega_0}(\omega_2)e^{-i\omega_1(t_f-x_B)}e^{-i\omega_2 x_A}[a_{\omega_1},a^\dagger_{\omega_2}] \\ &= \int_0^\infty d\omega \Lambda_{\omega_0}(\omega)F_{\omega_0}(\omega)e^{-i\omega t_f}e^{i\omega(x_B-x_A)}\,, \end{aligned} \tag{67}$$

and the commutator $[a_{\omega_1},a^\dagger_{\omega_2}]=\delta(\omega_1-\omega_2)$. The distance the photon travels in spacetime from Alice to Bob is given by

$$x_B-x_A=\left[(r_A-r_B)+2M\log\left(\frac{r_B-2M}{r_A-2M}\right)\right]\,, \tag{68}$$

where the first term (r_A-r_B) describes the propagation of the photon in flat space whereas the second term includes the contribution due to the curvature of space by the mass M. From the perspective of this formalism there is effectively only one clock - that of the asymptotic observer - and so, unlike the local formalism, the spectral distribution $F_{\omega_0}(\omega)$ of the wavepacket sent by Alice remains unaltered at the time and position of Bob's measurement. Moreover, the additional linear spectral phase contribution due to the curvature of space implies a shift in the time domain which can be easily compensated for by Bobs timing electronics. If this is done, Eq. (67) simply describes the signal of a single photon detection in a flat spacetime scenario.

The local formalism (Section VI B) in which there are two observers with locally defined clock rates is effectively equivalent to the global picture in the case that the spacetime is known and the redshift relation between the clocks can be determined. In particular the transformation between the two formalisms can be calculated

$$\begin{aligned}\psi_1(x_A;x_B,t_f) &= \int_0^\infty d\omega F_{\omega_0}(\omega)\Lambda_{\omega_0}(\omega)e^{-i\omega t_f}e^{i\omega(x_B-x_A)} \\ &= N_{OB}\int_0^\infty d\Omega_B F_{\omega_0}(N_{OB}\Omega_B)\Lambda_{\omega_0}(N_{OB}\Omega_B)e^{-i\Omega_B\tau_{Bf}}e^{iN_{OB}\Omega_B(x_B-x_A)} \\ &= N_{OB}\int_0^\infty d\Omega_B \frac{1}{\sqrt{N_O B}}F^B_{\Omega_{B0}}(\Omega_B)\frac{1}{\sqrt{N_O B}}\Lambda^B_{\Omega_{B0}}(\Omega_B)e^{-i\Omega_B\tau_{Bf}}e^{iN_{OB}\Omega_B(x_B-x_A)} \\ &= \int_0^\infty d\Omega_B \Lambda^B_{\Omega_{B0}}(\Omega_B)F^B_{\Omega_{B0}}(\Omega_B)e^{-i\Omega_B\tau_{Bf}}e^{i\Omega_B\tau_{B_{xB-xA}}}\,, \end{aligned} \tag{69}$$

where we used Eq. (46). We further obtained

$$\tau_{B_{xB-xA}}=N_{OB}(x_B-x_A)=\sqrt{V(r_B)}t_{x_B-x_A}\,. \tag{70}$$

This is consistent with the relation between the proper time τ and the Schwarzschild time coordinate t given by Eq. (4). The physical interpretation of Eq. (70) is the following: While $t_{xB-xA}=(x_B-x_A)$ with $c=1$

is the time the photon needs to travel from Alice to Bob measured by the asymptotic observer, Eq. (70) is the time of flight measured by the clock in Bobs reference frame. Consequently, the additional constant phase leads to a time-shift of the first-order correlation function. The latter is now centered at the time Bob reads on his clock when he detects the photon if, at the time of emission, the clocks of Alice and Bob are both synchronized.

Since the radial position of Alice and Bob has not been taken into account in the representation of the operators in Section V B 1 the first-order correlation function of Eq. (58) does not account for the additional time shift due to the time of flight of the photon from Alice to Bob. Eq. (58) implicitly corrects for this delay and is always centered around zero.

D. Energy-time entangled photons by type-II SPDC

Entanglement between photons [6] plays a key role in a variety of experiments ranging from fundamental studies of quantum mechanics [25] towards applied fields of research like quantum communication [3] or quantum imaging [26].

Entangled photons are commonly generated by spontaneous parametric down-conversion (SPDC) [27]. From an experimental point of view, this process is described in more detail in Section VIII C. The two photon states generated by SPDC reads

$$|\Psi_2\rangle = |0\rangle + \int_0^\infty d\omega_s \int_0^\infty d\omega_i \; \Lambda(\omega_s, \omega_i) \; a^\dagger_{\omega_s} a^\dagger_{\omega_i} |0\rangle \; , \tag{71}$$

where, the function $\Lambda(\omega_s, \omega_i)$ is denoted as the joint-spectral amplitude (JSA). The state of Eq. (71) is entangled since the JSA can in general *not* be written as $\Lambda(\omega_s, \omega_i) = g(\omega_s)h(\omega_i)$. Note, that the index s and i differentiates the photons with regard to another degree of freedom; for instance here their polarisation degree of freedom as outlined in VIII C. Since we have distinguishable photons the commutator reads

$$\left[a_{\omega_j}, a^\dagger_{\omega'_k}\right] = \delta_{jk}\delta(\omega_j - \omega'_k), \qquad j,k \in \{s,i\} \; , \tag{72}$$

and all other commutators are zero.

E. Second-order correlation function: Experimental scenario

We again consider the scenario where Alice and Bob are situated at two different heights in the gravitational potential of the Earth. Alice resides in her laboratory on the surface of the Earth at radial coordinate $r_A = r_E$ and Bob is on on a satellite located at a constant radius $r_B = r_E + h$ and having no angular motion with

respect to Alice (Fig.1). Alice generates energy-time entangled photon pairs by a type-II SPDC process as discussed in Section VI D. The photons are then deterministically separated by a polarizing beam splitter (PBS). The signal photon is detected by Alice whereas the idler photon is detected by Bob. The output of the detectors are time-tagged in order to perform coincidence detection. The detection of the two-photon state is formally described by a second-order correlation function [24] which represents the probability per unit (time)^2 that one photon is recorded at (x_1,t_1) and the other photon at (x_2,t_2). It is assumed that both parties use the same type of detector.

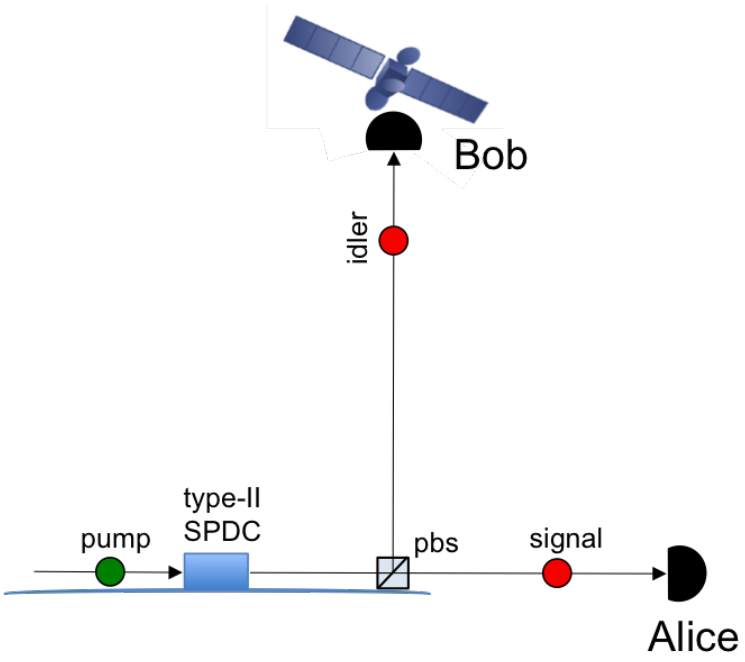

FIG. 2. Alice generates energy-time entangled two-photon states via type-II SPDC. The photons are separated by a PBS. The signal photon is detected by Alice whereas the idler photon is detected by Bob. Both detectors are connected in a coincidence circuit.

F. Second-order correlation function in local coordinates

We first work out the scenario shown in Fig. 2 in the local reference frames of Alice and Bob taking into account the properties and relations given in Section V B 1.

The type-II energy-time entangled two-photon state generated by SPDC in the local frame of Alice reads

$$|\Psi_2\rangle = \int_0^\infty d\Omega_{As} \int_0^\infty d\Omega_{Ai}\, \Lambda^A(\Omega_{As}, \Omega_{Ai}) a^\dagger_{\Omega_{As}} a^\dagger_{\Omega_{Ai}} |0\rangle. \tag{73}$$

Without loss of generality we calculate the second-order correlation function for an initial time $\tau_{Ai} = 0$ on the clock of Alice to be

$$\begin{aligned} G^{(2)}(x_A, \tau_{Af_1}; x_B\tau_{Bf_2}) &= \langle\Psi_2|\Pi^{(2)}(\tau_{Af_1}, \tau_{Bf2})|\Psi_2\rangle \\ &= \langle\Psi_2|a^\dagger(\tau_{Af_1})a^\dagger(\tau_{Bf_2})|0\rangle\langle 0|a(\tau_{Bf_2})a(\tau_{Af_1})|\Psi_2\rangle \\ &= |\psi_2(x_A, \tau_{Af_1}; x_B, \tau_{Bf_2})|^2 \,, \end{aligned} \tag{74}$$

where

$$\begin{aligned} &\psi_2\left(\tau_{Af_1}, \tau_{Bf_2}\right) = \langle 0|a(\tau_{Bf_2})a(\tau_{Af_1})|\Psi_2\rangle \\ &= \int_0^\infty d\Omega_{Bi}\int_0^\infty d\Omega'_{As}\int_0^\infty d\Omega_{Ai}\int_0^\infty d\Omega_{As}e^{-i(\Omega'_{As}\tau_{Af_1}+\Omega_{Bi}\tau_{Bf_2})}F^A_{\Omega_{A0}}(\Omega'_{As})F^B_{\Omega_{B0}}(\Omega_{Bi}) \\ &\times \Lambda^A(\Omega_{As}, \Omega_{Ai})[a_{\Omega'_{As}}, a^\dagger_{\Omega_{As}}][a_{\Omega_{Bi}}, a^\dagger_{\Omega_{Ai}}] \,, \end{aligned} \tag{75}$$

where the dependency on (x_A, x_B) is implicit in the definition of the proper times. We now use that

$$[a_{\Omega_{Bi}}, a^\dagger_{\Omega_{Ai}}] = \sqrt{N_{AB}}[a_{\Omega'_{Ai}}, a^\dagger_{\Omega_{Ai}}] = \sqrt{N_{AB}}\delta(\Omega'_{Ai} - \Omega_{Ai}) \,, \tag{76}$$

taking into account Eq. (44). Then

$$\begin{aligned} &\psi_2\left(\tau_{Af_1}, \tau_{Bf_2}\right) = \langle 0|a(\tau_{Bf_2})a(\tau_{Af_1})|\Psi_2\rangle \\ &= \sqrt{N_{AB}}\int_0^\infty d\Omega_{Bi}\int_0^\infty d\Omega'_{As}e^{-i(\Omega'_{As}\tau_{Af_1}+\Omega_{Bi}\tau_{Bf_2})}F^A_{\Omega_{A0}}(\Omega'_{As})F^B_{\Omega_{B0}}(\Omega_{Bi})\Lambda^A(\Omega'_{As}, \Omega'_{Ai}) \,. \end{aligned} \tag{77}$$

We now use Eq. (46) to write

$$\begin{aligned} \psi_2(\tau_{Af_1}, \tau_{Bf_2}) = N_{AB}\int_0^\infty d\Omega_{Bi}\int_0^\infty d\Omega'_{As}e^{-i(\Omega'_{As}\tau_{Af_1}+\Omega_{Bi}\tau_{Bf_2})} \\ \times F^A_{\Omega_{A0}}(\Omega'_{As})F^A_{\Omega_{A0}}(N_{AB}\Omega_{Bi})\Lambda^A(\Omega'_{As}, \Omega'_{Ai}) \,. \end{aligned} \tag{78}$$

With the invariant $\Omega_{Bi}\tau_{Bf_2} = \Omega'_{Ai}\tau_{Af_2}$ and the substitution $\Omega'_{Ai} = N_{AB}\Omega_{Bi}$, we finally obtain

$$\begin{aligned} \psi_2(\tau_{Af_1}, \tau_{Bf_2}) = \int_0^\infty d\Omega'_{As}\int_0^\infty d\Omega'_{Ai}e^{-i(\Omega'_{As}\tau_{Af_1}+\Omega'_{Ai}\tau_{Af_2})}F^A_{\Omega_{A0}}(\Omega'_{As})F^A_{\Omega_{A0}}(\Omega'_{Ai}) \\ \times\Lambda^A(\Omega'_{As}, \Omega'_{Ai}) \,. \end{aligned} \tag{79}$$

We can simplify this expression further for the case of a CW pump field where

$$\Lambda^A(\Omega'_{As}, \Omega'_{Ai}) = \delta(\Omega_{cp} - \Omega'_{As} - \Omega'_{Ai})\Phi^A(\Omega'_{As}, \Omega'_{Ai}) \,. \tag{80}$$

Then

$$\psi(\tau_{Af_1}, \tau_{Bf_2}) = \mathrm{e}^{-i\Omega_{cp}\tau_{Bf2}}\int d\Omega'_{As}e^{-i\left[\Omega'_{As}(\tau_{Af_1}-\tau_{Af2})\right]}F^A_{\Omega_{A0}}(\Omega'_{As})F^A_{\Omega_{A0}}(\Omega_{cp} - \Omega'_{As})\Phi^A(\Omega'_{As}). \tag{81}$$

1. Fidelity

In Section VI B 1 we discussed the fidelity in the context of a first-order correlation function. Here, we apply this quantity to the scenario shown in Fig. 2. By doing so, we first define $|\Psi_2^{AA}\rangle \doteq |\Psi_2\rangle$ and we extend the notation of the JSA to $\Lambda^A \rightarrow \Lambda^{AA}$. We then analogously have

$$|\Psi_2^{AB}\rangle = \int_0^\infty d\Omega_{As} \int_0^\infty d\Omega_{Bi}\, \Lambda^{AB}(\Omega_{As}, \Omega_{Bi}) a^\dagger_{\Omega_{As}} a^\dagger_{\Omega_{Bi}} |0\rangle, \tag{82}$$

where the relation of Eq. (46) is applied to the JSA according to

$$\Lambda^{AB}(\Omega_{As}, \Omega_{Bi}) = \sqrt{N_{AB}} \Lambda^{AA}(\Omega_{As}, N_{AB}\Omega_{Bi}) \tag{83}$$

taking into account the redshift experienced by the idler photon due to its propagation from the local frame of Alice to the local frame ob Bob. The fidelity $F^B = |\Delta^B|^2$ evaluated in Bob's reference frame is then expressed in terms of

$$\begin{aligned}
\Delta^B &= \langle \Psi_2^{AB} | \Psi_2^{AA} \rangle \\
&= \int_0^\infty d\Omega_{As} \int_0^\infty d\Omega_{Ai} \int_0^\infty d\Omega'_{As} \int_0^\infty d\Omega_{Bi}\, \Lambda^{AA}(\Omega_{As}, \Omega_{Ai}) \bar{\Lambda}^{AB}(\Omega'_{As}, \Omega_{Bi}) \\
&\times \langle 0 | a_{\Omega'_{As}} a_{\Omega_{Bi}} a^\dagger_{\Omega_{As}} a^\dagger_{\Omega_{Ai}} |0\rangle \\
&= \int_0^\infty d\Omega_{Bs} \int_0^\infty d\Omega'_{Bi} \int_0^\infty d\Omega'_{Bs} \int_0^\infty d\Omega_{Bi}\, \underbrace{\sqrt{N_{AB}} \sqrt{N_{AB}} \Lambda^{AA}(N_{AB}\Omega_{Bs}, N_{AB}\Omega'_{Bi})}_{=\Lambda^{BB}(\Omega_{Bs}, \Omega'_{Bi})} \\
&\times \underbrace{\sqrt{N_{AB}} \bar{\Lambda}^{AB}(N_{AB}\Omega'_{Bs}, \Omega_{Bi})}_{=\bar{\Lambda}^{BB}(\Omega'_{Bs}, \Omega_{Bi})} \delta(\Omega'_{Bs} - \Omega_{Bs}) \delta(\Omega_{Bi} - \Omega'_{Bi}) \\
&= \int_0^\infty d\Omega_{Bs} \int_0^\infty d\Omega_{Bi}\, |\Lambda^{BB}(\Omega_{Bs}, \Omega_{Bi})|^2 \\
&= 1
\end{aligned} \tag{84}$$

under the assumption of a normalized JSA. We have further used the operator relation $a_{\Omega_A} = 1/\sqrt{N_{AB}} a_{\Omega_B}$. As for the first-order correlation, the fidelity is unity if the known redshift factor is taken into account by Bob. Again we do not consider the additional linear spectral phase due to the propagation of the idler photon since it will not play any role for the spectral measurement. It can be shown, that the same result as in Eq. 84 can be obtained by expressing the fidelity in the reference frame of Alice using the inverse redshift transformation relations, i.e.

$$\begin{aligned}\Delta^A &= \langle \Psi_2^{AB} | \Psi_2^{AA} \rangle \\ &= \int_0^\infty d\Omega_{As} \int_0^\infty d\Omega_{Ai} \, |\Lambda^{AA}(\Omega_{As}, \Omega_{Ai})|^2 \\ &= 1. \end{aligned} \tag{85}$$

For an SPDC state Eq. (61) reads

$$\Delta = \int_0^\infty d\Omega \int_0^\infty d\Omega' \, \bar{\Lambda}^{AB}(\Omega, \Omega') \Lambda^{AA}(\Omega, \Omega') \tag{86}$$

and reduces to

$$\Delta = \int_0^\infty d\Omega \, \bar{\Phi}^{AB}(\Omega, -\Omega) \Phi^{AA}(\Omega, -\Omega) \tag{87}$$

for a monochromatic pump approximation. By means of Eq. (87) we calculate $F = |\Delta|^2 \sim 1 - 1 \times 10^{-15}$ for a 532 nm $\rightarrow$ 1064 nm SPDC state expressed in a double Gaussian model with a spectral bandwidth of 42 nm (FWHM) [28]. The double Gaussian model applied here is for simplicity formulated for a type-I SPDC where the signal and idler photon experience the same refractive index while propagating through the non-linear crystal. However, the value of the fidelity is expected not to be altered considering a type-II process which is the primary SPDC process considered in this report (see Section VI D and VIII C).

G. Second-order correlation function in Schwarzschild coordinates

We now calculate the second-order correlation function corresponding to the experimental scenario in Fig. (2), but taking the asymptotic observer perspective outlined at the beginning of Section VI C. The type-II energy-time entangled two-photon state generated by SPDC in the lab of Alice reads

$$|\Psi_2\rangle = \int_0^\infty d\omega_s \int_0^\infty d\omega_i \, \Lambda(\omega_s, \omega_i) \, a^\dagger_{\omega_s} a^\dagger_{\omega_i} |0\rangle \, , \tag{88}$$

where we have omitted the leading order vacuum contribution. Note, that the state is implicitly produced at the initial time $t_i = 0$. Further, the radial position x_A of its creation does not appear in Eq. (88) taking into account the standard derivation of the two-photon state outlined in Section VI D. To adapt the state to the framework considered here, we rewrite Eq. (88) as

$$|\Psi_2\rangle = \int_0^\infty d\omega_s \int_0^\infty d\omega_i \, \Lambda(\omega_s, \omega_i) \mathrm{e}^{-i(\omega_s + \omega_i)x_A} a^\dagger_{\omega_s} a^\dagger_{\omega_i} |0\rangle \, , \tag{89}$$

where we have included an additional phase depending on the radial positions. After the PBS the idler photon is sent to the detector of Bob whose photon detection at final time t_{f2} is described by the annihilation operator

$$a_{\omega_0}(x_B, t_{f2}) = \int_0^\infty d\omega_i F_{\omega_0}(\omega_i) \mathrm{e}^{i\omega_i(x_B - t_{f2})} a_{\omega_i} \ , \tag{90}$$

and Alice detects the signal photon at final time t_{f1} via

$$a_{\omega_0}(x_A, t_{f1}) = \int_0^\infty d\omega_s F_{\omega_0}(\omega_s) \mathrm{e}^{i\omega_s(x_A - t_{f1})} a_{\omega_s} \ . \tag{91}$$

As indicated in Section VI E both detectors have the same spectral response function $F_{\omega_0}(\omega)$. We can now work out the second-order correlation function in the reference frame of the asymptotic observer as

$$\begin{aligned} G^{(2)}(x_A, t_{f1}; x_B, t_{f2}) &= \langle \Psi_2 | \Pi^{(2)}(x_A, t_{f1}; x_B, t_{f2}) | \Psi_2 \rangle \\ &= \langle \Psi_2 | a^\dagger_{\omega_0}(x_A, t_{f1}) a^\dagger_{\omega_0}(x_B, t_{f2}) | 0 \rangle \langle 0 | a_{\omega_0}(x_B, t_{f2}) a_{\omega_0}(x_A, t_{f1}) | \Psi_2 \rangle \\ &= |\psi(x_A, t_{f1}; x_B, t_{f2})|^2 \ , \end{aligned} \tag{92}$$

where the two-photon wave function reads

$$\begin{aligned} \psi_2(x_A, t_{f1}; x_B, t_{f2}) = \int_0^\infty d\omega_s \int_0^\infty d\omega_i \ \Lambda(\omega_s, \omega_i) F_{\omega_0}(\omega_s) F_{\omega_0}(\omega_i) \mathrm{e}^{-i(\omega_s + \omega_i)x_A} \mathrm{e}^{i\omega_s x_A} \mathrm{e}^{i\omega_i x_B} \\ \times \ \mathrm{e}^{-i\omega_s t_{f1}} \mathrm{e}^{-i\omega_i t_{f2}} \ . \end{aligned} \tag{93}$$

We now use the approximation of the JSA for a CW pumped SPDC process

$$\Lambda(\omega_s, \omega_i) = \delta(\omega_{cp} - \omega_s - \omega_i) \Phi(\omega_s, \omega_i) \ , \tag{94}$$

to obtain

$$\psi_2(x_A, t_{f1}; x_B, t_{f2}) = \psi_2(x_A; x_B, t_{f2} - t_{f1}) \propto \int_0^\infty d\omega \ \Phi(\omega) F_{\omega_0}(\omega) F_{\omega_0}(\omega) \mathrm{e}^{i\omega(x_A - x_B)} \mathrm{e}^{-i\omega(t_{f2} - t_{f1})}, \tag{95}$$

where we define $\Phi(\omega) = \Phi(\omega, \omega_{cp} - \omega)$. The phase factor introduced in Eq. (89) results in a global phase for a CW pump field. If we set $x_A = x_B$ we obtain

$$\psi_2(t_{f2} - t_{f1}) \propto \int_0^\infty d\omega \ \Phi(\omega) F_{\omega_0}(\omega) F_{\omega_0}(\omega) \mathrm{e}^{-i\omega(t_{f2} - t_{f1})} \ , \tag{96}$$

which coincides with the result obtained by performing a standard *flat* spacetime calculation of the temporal second-order correlation function (see for instance the result of Eq. (10.36) in [20]) for which both detectors are at the same z-distance from the source. Similarly, by setting $M = 0$ and $x_A \neq x_B$, one also obtains the

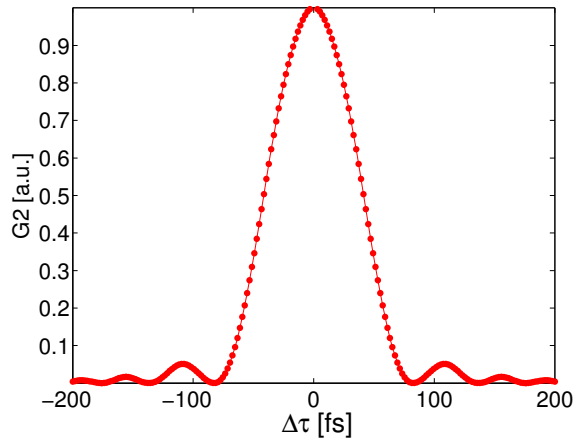

FIG. 3. Eq. (97) for $r_A = r_B$.

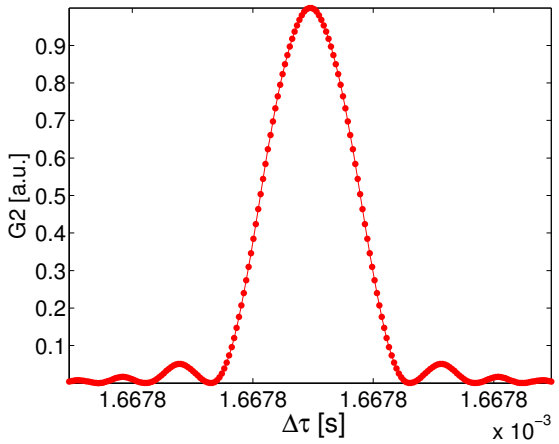

FIG. 4. Eq. (97) for $r_A = r_E$ and $r_B = r_E + 500\,\text{km}$.

flat spacetime limit.

In order to get numerical results we first rewrite Eq. (95) as

$$\psi(r_A; r_B, t_{f2} - t_{f1}) \propto \int_0^\infty d\omega\ \Phi(\omega) F_{\omega_0}(\omega) F_{\omega_0}(\omega) \mathrm{e}^{i\frac{\omega}{c}\left[(r_A - r_B) + \frac{2GM}{c^2}\log\left(\frac{r_A c^2 - 2GM}{r_B c^2 - 2GM}\right)\right]} \mathrm{e}^{-i\omega(t_{f2} - t_{f1})}\,, \tag{97}$$

using SI units and we further define $\Delta\tau = t_{f2} - t_{f1}$. This time shift describes the propagation time a photon needs to travel from Alice to Bob in a curved spacetime and is given explicitly by

$$t_{shift} = c^{-1}\left[(r_A - r_B) + \frac{2GM}{c^2}\log\left(\frac{r_A c^2 - 2GM}{r_B c^2 - 2GM}\right)\right]\,. \tag{98}$$

The first contribution $c^{-1}(r_A - r_B)$ describes the light propagation in flat spacetime whereas the second contribution includes the curvature of the spacetime induced by the mass M. If Bob is situated at a LEO altitude of $500\,\text{km}$, the latter contribution is on the order of picoseconds. Figure 3 shows a second-order correlation function with Eq. (96) as the two-photon wave function, i.e. we consider the case $r_A = r_B$. Figure 4 shows the second-order correlation function using the two-photon wave function from Eq. (97) with Bob again on a satellite in LEO $r_B = r_E + 500\,\text{km}$. As expected, the correlation function is just shifted by the amount of t_{shift} without altering its shape.

Note that in the simulation, as is often the convention, we assume $F_{\omega_0}(\omega) = 1$ and we use the phase-matching function of Eq. (151) optimized for $532\,\text{nm} \to 1064\,\text{nm}$ SPDC. In this case we have

$$\Phi(\omega) = \mathrm{sinc}\left(\frac{\Delta k_z(\omega) L}{2}\right)\,, \tag{99}$$

where L is the length of the non-linear crystal and $\Delta k_z(\omega)$ is the longitudinal phase mismatch (see Section VIII C for further details.) As in Section VI C we now reformulate Eq. (93) in a local coordinate system.

For this we make use of the relations $\omega_s = N_{OA}\Omega_{As}$ and $\omega_i = N_{OA}\Omega_{Ai}$ to obtain

$$\begin{aligned}\psi_2(x_A, t_{f1}; x_B, t_{f2}) &= \int_0^\infty d\omega_s \int_0^\infty d\omega_i\ \Lambda(\omega_s, \omega_i) F_{\omega_0}(\omega_s) F_{\omega_0}(\omega_i) \mathrm{e}^{-i(\omega_s+\omega_i)x_A} \mathrm{e}^{i\omega_s x_A} \mathrm{e}^{i\omega_i x_B} \\ &\times \mathrm{e}^{-i\omega_s t_{f1}} \mathrm{e}^{-i\omega_i t_{f2}} \\ &= \int_0^\infty d\Omega_{As} \int_0^\infty d\Omega_{Ai}\ N_{OA}\Lambda(N_{OA}\Omega_{As}, N_{OA}\Omega_{Ai}) \sqrt{N_{OA}} F_{\omega_0}(N_{OA}\Omega_{As}) \sqrt{N_{OA}} F_{\omega_0}(N_{OA}\Omega_{Ai}) \\ &\times \mathrm{e}^{-i(\Omega_{As}+\Omega_{Ai})N_{OA}x_A} \mathrm{e}^{i\Omega_{As}N_{OA}x_A} \mathrm{e}^{i\Omega_{Ai}N_{OA}x_B} \mathrm{e}^{-i\Omega_{As}\tau_{Af1}} \mathrm{e}^{-i\Omega_{Ai}\tau_{Bf2}} \\ &= \int_0^\infty d\Omega_{As} \int_0^\infty d\Omega_{Ai}\ \Lambda^A(\Omega_{As}, \Omega_{Ai}) F^A_{\Omega_{A0}}(\Omega_{As}) F^A_{\Omega_{A0}}(\Omega_{Ai}) \\ &\times \mathrm{e}^{-i(\Omega_{As}+\Omega_{Ai})\tau_{A_{xA}}} \mathrm{e}^{i\Omega_{As}\tau_{A_{xA}}} \mathrm{e}^{i\Omega_{Ai}\tau_{A_{xB}}} \mathrm{e}^{-i\Omega_{As}\tau_{Af1}} \mathrm{e}^{-i\Omega_{Ai}\tau_{Bf2}}\ . \end{aligned} \tag{100}$$

Here, we used $\tau_{A_{xA}} = N_{OA}x_A$ and $\tau_{A_{xB}} = N_{OA}x_B$ in analogy to Eq. (70). As with the first order correlation functions, when the spacetime, and the transformation between clocks, is known to both observers, there is effectively only one reference frame in play and the local/global formalisms are equivalent (up to some phase factors). If, on the other hand, we assume that the observers do not account for curvature effects then, as with the fidelity, there will be non-trivial differences that are ultimately rooted in gravitational redshift effects on the pulse shapes and arrival times. The similar behaviour, for the propagation from Alice to Bob, of a single photon or two photons from a pair expected from standard quantum mechanics, as the considered setup and the corresponding observable are not sensitive to entanglement. Within the framework of standard quantum theory, and of QFTCS, the same second-order temporal correlation functions would be obtained with mixed states showing the same temporal correlations as the entangled states. This is why a set of measurements in various bases is required to prove entanglement, for instance by performing high resolution temporal and spectral measurements, which is in practice very difficult. The next section introduces a scheme based on interferometric measurements, that is commonly used to test entanglement in the time-energy domain.

VII. The Franson experiment

A. Experimental framework

A scheme to analyze energy-time entangled two-photon states was proposed by Franson in 1989 (Figure 5) [29]. The source considered consists of a SPDC process where a pump photon of an intense laser field is spontaneously converted into a pair of entangled photons in a NLC. The pump field is considered here as a classical field of a CW laser having a central frequency ω_{cp} and a narrow spectral bandwidth $\Delta\omega_p$.[1] Although each of the down-converted photons can have a considerably large bandwidth $\Delta\omega_{s,i} \doteq \Delta\omega_s =$

[1] For a typical CW laser the bandwidth could be < 5 MHz or expressed in wavelength < 5 fm in full width at half maximum.

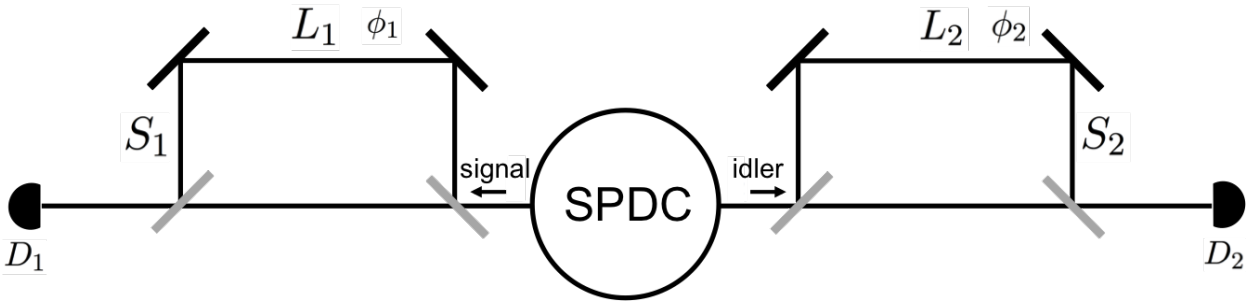

FIG. 5. A photon pair is generated by SPDC within the coherence time of a pump photon τ_p^{coh}. Both photons are then injected into two separated Mach-Zehnder interferometers (MZIs) with variable path lengths. All involved beamsplitters are assumed to be 50% in reflection and transmission. Possible phases ϕ_1 and ϕ_2 are accumulated due to the beamsplitters and mirrors. The detectors D_1 and D_2 are connected in coincidence.

$\Delta\omega_i$ compared to the pump bandwidth their sum in frequency is constrained by energy conservation and therefore fixed within the bandwidth of the pump.[2] Thus the frequencies (ω_s,ω_i) of the photon pair are constrained by

$$\omega_s + \omega_i = \omega_p \in [\omega_{cp} - \Delta\omega_p/2, \omega_{cp} + \Delta\omega_p/2], \tag{101}$$

where we choose the experimental conditions such that the central frequency of the generated photons is given by $\omega_c \doteq \omega_{cs} = \omega_{ci} = \omega_{cp}/2$. The very small bandwidth of the pump guarantees a highly energy-time entangled state with a Schmidt number on the order of 10^6, the latter quantifying the degree of entanglement of a pure bipartite state [30].

The entangled photons not only show correlations in energy moreover they are also strongly correlated in time. While the correlation in frequency is determined by the small bandwidth of the pump, the correlation in time is defined by the large bandwidth $\Delta\omega_{s,i}$ of the down-converted photons: This bandwidth determines the temporal coherence (or entanglement) time $\tau_{s,i}^{coh} \propto \frac{1}{\Delta\omega_{s,i}}$ to be of the order of fs. From this it follows that if one photon is detected at time t the other photon will be detected within $\tau_{s,i}^{coh}$, i.e. both photons are created almost simultaneously within the NLC. Since the difference in the time of emission of the photons is close to zero and their frequencies are correlated we have simultaneous correlations in time *and* frequency which is *the* property of energy-time entanglement, which no classically correlated state can possess. More formally, we almost have

$$\Delta(t_1 - t_2) = 0,$$
$$\Delta(\Omega_s + \Omega_i) = 0,$$

[2] A typical bandwidth for SPDC photons is ∼100 nm.

where on the other hand we have $\Delta t_1, \Delta t_2 >> 1$ and $\Delta\omega_s, \Delta\omega_i >> 1$. Here we introduced the relative frequency defined by $\Omega_j = \omega_j - \omega_c$ and Δ denotes the statistical uncertainty (standard deviation). On the other hand, the creation time of each photon is highly uncertain due to the large coherence time of the pump $\tau_p^{coh} \propto \frac{1}{\Delta\omega_p} >> 1$. Therefore we are faced with the situation that although the time of birth of each photon within the NLC is highly undetermined, the joint-temporal-detection of the photons reveals almost perfect correlation.

B. Second-order correlation function in a flat spacetime

If the optical imbalance $\Delta L_j = L_j - S_j$ of the path lengths of interferometer $j = 1, 2$ is below the coherence length $c\tau_{s,i}^{coh}$ of the individual photons, single photon interference fringes will appear in a first-order intensity measurement at detector D_j if the corresponding optical imbalance is altered. The fringes will have a periodicity related to the wavelength of the individual photons and a corresponding second-order correlation signal will consist of the product of two independent single photon interference rates. This contribution to the coincidence signal should be suppressed and therefore we assume ΔL_1 and ΔL_2 to be much larger than $c\tau_{s,i}^{coh}$, which is experimentally feasible since already at an imbalance of $\approx$100 μm this condition is fulfilled. In the following, we further assume all reflection and transmission coefficients of the involved beamsplitters to be $1/2$.

To start the calculation we first consider the photon annihilation operators at the position of the detectors D_1 and D_2. For D_1 it reads

$$\begin{aligned} a_1(S_1, L_1, t_1) &= \frac{1}{2} a_s(S_1, t_1) + \frac{1}{2} \mathrm{e}^{i\phi_1} a_s(L_1, t_1) \\ &= \frac{1}{2} \int d\omega_s \, \mathrm{e}^{ik(\omega_s)S_1 - i\omega_s t_1} a_{\omega_s} + \frac{1}{2} \mathrm{e}^{i\phi_1} \int d\omega_s \, , \mathrm{e}^{ik(\omega_s)L_1 - i\omega_s t_1} a_{\omega_s} \, , \end{aligned} \tag{102}$$

and similarly for D_2

$$\begin{aligned} a_2(S_2, L_2, t_2) &= \frac{1}{2} a_i(S_2, t_2) + \frac{1}{2} \mathrm{e}^{i\phi_2} a_i(L_2, t_2) \\ &= \frac{1}{2} \int d\omega_i \, \mathrm{e}^{ik(\omega_i)S_2 - i\omega_i t_2} a_{\omega_i} + \frac{1}{2} \mathrm{e}^{i\phi_2} \int d\omega_i \, , \mathrm{e}^{ik(\omega_i)L_2 - i\omega_i t_2} a_{\omega_i} \, , \end{aligned} \tag{103}$$

where S_j and L_j are the longitudinal coordinates along the optical path from the source to the detector and we assume that the distance of additional free-space propagation distances outside the MZI are the same for both photons and do therefore not alter the coincidence signal. The times t_j are the absolute times at the detectors and ϕ_j are potential phases introduced by the beam-splitters and mirrors. The dispersion relation for free-space propagation of a photon is given by $k(\omega_j) = \frac{\omega_j}{c}$. Note, that in the flat spacetime scenario we do, for simplicity, not take into account a spectral response function $F(\omega)$ of the detection device. We

consider here again a SPDC process of type-II. Therefore, the signal and idler photons are distinguishable and separated by a PBS due to their orthogonal polarization. As a consequence, the commutator of Eq. (72) also holds in the following considerations. The second-order correlation function is then given by

$$\begin{aligned} G^{(2)}(S_1, L_1, t_1; S_2, L_2, t_2) &= \langle \Psi_2 | a_1^\dagger a_2^\dagger a_2 a_1 \, | \Psi_2 \rangle \\ &= |\psi_2(S_1, L_1, t_1; S_2, L_2, t_2)|^2 \, , \end{aligned} \tag{104}$$

using the operators of Eq. (102) and Eq. (103). The effective coincidence rate is expressed as

$$R_c \propto \frac{1}{T_c} \int_0^{Tc} dt_1 \int_0^{Tc} dt_2 \, G^{(2)}(S_1, L_1, t_1; S_2, L_2, t_2) \, , \tag{105}$$

with a coincidence window having a temporal width T_c [31]. The two-photon wave function reads

$$\begin{aligned} \psi_2(S_1, L_1, t_1; S_2, L_2, t_2) = \frac{1}{4} \big\{ & \langle 0 | a_i(S_2, t_2) a_s(S_1, t_1) \, | \Psi_2 \rangle + \mathrm{e}^{i\phi_1} \langle 0 | a_i(S_2, t_2) a_s(L_1, t_1) \, | \Psi_2 \rangle \\ & + \mathrm{e}^{i\phi_2} \langle 0 | a_i(L_2, t_2) a_s(S_1, t_1) \, | \Psi_2 \rangle + \mathrm{e}^{i(\phi_1+\phi_2)} \langle 0 | a_i(L_2, t_2) a_s(L_1, t_1) \, | \Psi_2 \rangle \big\} \\ = \frac{1}{4} \big\{ & \psi_2(S_1, t_1; S_2, t_2) + \mathrm{e}^{i\phi_1} \psi_2(L_1, t_1; S_2, t_2) \\ & + \mathrm{e}^{i\phi_2} \psi_2(S_1, t_1; L_2, t_2) + \mathrm{e}^{i(\phi_1+\phi_2)} \psi_2(L_1, t_1; L_2, t_2) \big\} \, , \end{aligned} \tag{106}$$

and involves all the contributing amplitudes for a coincidence event: The photons can take their paths according to (S,S), (S,L), (L,S), (L,L). Remember that we assumed the path length difference of both MZI to obey the condition $\Delta L_1, \Delta L_2 >> c\tau_{s,i}^{coh}$. This implies for the (S,L), (L,S) events that the relative arrival time difference for the two photons is large compared to their individual coherence time, which makes them distinguishable at the position of the detectors. Since distinguishable events do not interfere, these events only contribute a constant background to the total coincidence signal. Experimentally, they can be discarded if the time of the coincidence window T_c is smaller than $(L_1 - S_2)/c$ and $(L_2 - S_1)/c$.

Further, in order that the (S,S) and (L,L) events are not distinguishable, it must be guaranteed that $\Delta L_1 - \Delta L_2 << c\tau_{s,i}^{coh}$. Finally, to guarantee that the (S,S) and (L,L) events are between photon pairs of indistinguishable SPDC events within the coherence time of the pump, it must hold that $\Delta L_1 + \Delta L_2 << c\tau_p^{coh}$. In this case, both photons of a pair created at an earlier time during the pump pulse and taking the long paths can not be distinguished from two photons created at a later time within the pump pulse and taking the short interferometer arms. We see interference between these events as long as the aforementioned condition is fulfilled. This agrees with the observation we made in Section VII A that the time of emission of a pair is uncertain within the coherence time of the pump. If the last condition is violated, the (S,S) and (L,L) can be attributed to two different SPDC processes originating from different pump pulses. No interference between

these two events is then possible. We therefore assume all these constraints to be realized and focus now on the calculation of the coincidence signal in the form of

$$\begin{aligned} R_c &\propto \frac{1}{T_c}\int_0^{T_c} dt_1 \int_0^{T_c} dt_2 |\psi_2(S_1,t_1;S_2,t_2) + \mathrm{e}^{i(\phi_1+\phi_2)}\psi_2(L_1,t_1;L_2,t_2)|^2 \\ &= \frac{1}{T_c}\int_0^{T_c} dt_1 \int_0^{T_c} dt_2 \{|\psi_2(S_1,t_1;S_2,t_2)|^2 + |\psi_2(L_1,t_1;L_2,t_2)|^2 \\ &+ \mathrm{e}^{i(\phi_1+\phi_2)}\psi_2(L_1,t_1;L_2,t_2)\psi_2^*(S_1,t_1;S_2,t_2) + \mathrm{e}^{-i(\phi_1+\phi_2)}\psi_2(S_1,t_1;S_2,t_2)\psi_2^*(L_1,t_1;L_2,t_2)\} \, . \end{aligned} \tag{107}$$

We consider a type-II SPDC state according to Eq. (88) approximated for a CW pump field, i.e.

$$|\Psi_2\rangle = \int d\omega \, \Phi(\omega) \, |1_\omega\rangle |1_{\omega_{cp}-\omega}\rangle \, . \tag{108}$$

This implies that $\tau_p^{coh} \to \infty$ and thus it is assumed that experimentally the condition $\Delta L_1 + \Delta L_2 << c\tau_p^{coh}$ is realized. Since it must hold that $|\langle\Psi_2|\Psi_2\rangle|^2 = 1$ we must have

$$\int d\omega \, |\Phi(\omega)|^2 = 1 \, . \tag{109}$$

For the two-photon wavefunction we explicitly obtain

$$\begin{aligned} \psi_2(X_1,t_1;X_2,t_2) &= \langle 0|a_i(X_2,t_2)a_s(X_1,t_1)|\Psi\rangle \\ &= \int d\omega \, \Phi(\omega) \, \mathrm{e}^{ik(\omega)X_1 - i\omega t_1} \, \mathrm{e}^{ik(\omega_{cp}-\omega)X_2 - i(\omega_{cp}-\omega)t_2} \\ &= \mathrm{e}^{-i\omega_{cp}t_2} \int d\omega \, \Phi(\omega) \, \mathrm{e}^{ik(\omega)X_1} \, \mathrm{e}^{ik(\omega_{cp}-\omega)X_2} \mathrm{e}^{-i\omega(t_1-t_2)} \, , \end{aligned} \tag{110}$$

for $X \in \{S, L\}$. The integration over the detection times yields

$$\begin{aligned} \frac{1}{T_c}\int_0^{T_c} dt_1 \int_0^{T_c} dt_2 \, |\psi(X_1,t_1;X_2,t_2)|^2 &= \frac{1}{T_c}\int_0^{T_c} dt_1 \int_0^{T_c} dt_2 \int d\omega \int d\omega' \, \Phi(\omega)\Phi^*(\omega') \\ &\times \mathrm{e}^{i(k(\omega)-k(\omega'))X_1} \, \mathrm{e}^{i(k(\omega_{cp}-\omega)-k(\omega_{cp}-\omega'))X_2} \, \mathrm{e}^{-i(\omega-\omega')(t_1-t_2)} \\ &= \int d\omega \int d\omega' \, \Phi(\omega)\Phi^*(\omega') \\ &\times \mathrm{e}^{i(k(\omega)-k(\omega'))X_1} \, \mathrm{e}^{i(k(\omega_{cp}-\omega)-k(\omega_{cp}-\omega'))X_2} \\ &\times \frac{1}{T_c}\int_0^{T_c} dt_1 \int_0^{T_c} dt_2 \mathrm{e}^{-i(\omega-\omega')(t_1-t_2)} \, . \end{aligned} \tag{111}$$

Next, we consider the integration

$$\begin{aligned} \frac{1}{T_c}\int_0^{T_c} dt_1 \int_0^{T_c} dt_2 \mathrm{e}^{-i(\omega-\omega')(t_1-t_2)} &= T_c \, \mathrm{sinc}^2\left[T_c(\omega-\omega')/2\right] \\ &= \pi \left(\frac{T_c}{\pi} \, \mathrm{sinc}^2\left[T_c(\omega-\omega')/2\right]\right) \, , \end{aligned} \tag{112}$$

where we used $\mathrm{sinc}(x) = \sin(x)/x$. Next note that the term in brackets is a representation of the Dirac-delta function

$$\lim_{T_c\to\infty}\left(\frac{T_c}{\pi}\mathrm{sinc}^2\left[T_c(\omega-\omega')/2\right]\right) = \delta(\omega-\omega')\ . \tag{113}$$

The limit of $T_c \to \infty$ is reasonable since we have $\tau_{s,i}^{coh}$ ∼fs and T_c ∼ns. In this limit we therefore obtain for Eq. (111) the result

$$\lim_{T_c\to\infty}\left(\frac{1}{T_c}\int_0^{T_c} dt_1\int_0^{T_c} dt_2\,|\psi(X_1,t_1;X_2,t_2)|^2\right) = \pi\int d\omega\,|\Phi(\omega)|^2 = \pi\ , \tag{114}$$

where we used Eq. (109). The first non-constant term in Eq. (107) is calculated to be

$$\begin{aligned} A_1 &= \mathrm{e}^{i(\phi_1+\phi_2)}\frac{1}{T_c}\int_0^{T_c} dt_1\int_0^{T_c} dt_2\,\psi(L_1,t_1;L_2,t_2)\psi^*(S_1,t_1;S_2,t_2)\\ &= \mathrm{e}^{i(\phi_1+\phi_2)}\mathrm{e}^{i\frac{\omega_{cp}}{c}(L_2-S_2)}\frac{1}{T_c}\int_0^{T_c} dt_1\int_0^{T_c} dt_2\left[\int d\omega\,\Phi(\omega)\mathrm{e}^{i\frac{\omega}{c}(L_1-L_2)}\mathrm{e}^{-i\omega(t_1-t_2)}\right]\\ &\times\left[\int d\omega'\,\Phi^*(\omega')\mathrm{e}^{-i\frac{\omega'}{c}(S_1-S_2)}\mathrm{e}^{i\omega'(t_1-t_2)}\right]\ . \end{aligned} \tag{115}$$

Again commuting the dt with the $d\omega$ integrals and using Eqs. (112, 113, 114) we find

$$A_1 = \pi\mathrm{e}^{i(\phi_1+\phi_2)}\mathrm{e}^{i\frac{\omega_{cp}}{c}(L_2-S_2)}\int d\omega\,|\Phi(\omega)|^2\mathrm{e}^{i\frac{\omega}{c}(\Delta L_1-\Delta L_2)}\ . \tag{116}$$

The last term of Eq. (107) is the complex conjugate of A_1, and so we obtain for the coincidence rate

$$R_c \propto \frac{1}{2}\left[1+Re\left\{\mathrm{e}^{i(\phi_1+\phi_2)}\mathrm{e}^{i\frac{\omega_{cp}}{c}\Delta L_2}\int d\omega\,|\Phi(\omega)|^2\mathrm{e}^{i\frac{\omega}{c}(\Delta L_1-\Delta L_2)}\right\}\right]\ , \tag{117}$$

where we have a maximal visibility of one, and as defined earlier $\Delta L_i = L_i - S_i$. Note, that the proportionality factor involves $\eta_1\eta_2$, i.e. the efficiencies of the detectors. For a simultaneous variation in the optical path differences $\Delta L_1 = \Delta L_2 = \Delta L$ one obtains

$$R_c \propto \frac{1}{2}\left[1+\cos\left(\frac{\omega_{cp}}{c}\Delta L+(\phi_1+\phi_2)\right)\right]\ . \tag{118}$$

The oscillation in the pump frequency with 100% visibility implies the coherent superposition of the probability amplitudes at two different pair emission times within the coherence time of the pump field. For variations in the optical path lengths with $\Delta L_1 \neq \Delta L_2$ we still have oscillations with ω_{cp}, however, their visibility is shaped according to

$$V(\Delta L_1,\Delta L_2) = \int d\omega\,|\Phi(\omega)|^2\mathrm{e}^{i\frac{\omega}{c}(\Delta L_1-\Delta L_2)}\ . \tag{119}$$

For highly broadband SPDC, Eq. (119) would be proportional to $\delta(\Delta L_1 - \Delta L_2)$ and thus a slight misalignment $\Delta L_1 \neq \Delta L_2$ would reduce the visibility to zero. On the other hand, a very narrowbanded spectrum

leads to a visibility close to one no matter of ΔL_1 and ΔL_2.

We show in Fig. (6) the coincidence rate according to Eq. (117) where the entangled photons have a central wavelength $\lambda_c = 1064\,\text{nm}$ and a bandwidth of $\Delta\lambda_{s,i} = 100\,\text{nm}$. This results in a coherence time of $\tau_{s,i}^{coh} \approx 17\,\text{fs}$ and consequently a coherence length of $l_{s,i}^{coh} \approx 5\,\mu\text{m}$. Fig. (6) shows oscillations at ω_{cp} modulated in visibility by the envelope function of Eq. (119), the latter having a width determined by $l_{s,i}^{coh}$. Note, that in the configuration considered here, interferometer one is fixed with a path length difference of $\Delta L_1 = 100\,\mu\text{m}$ while ΔL_2 is scanned.

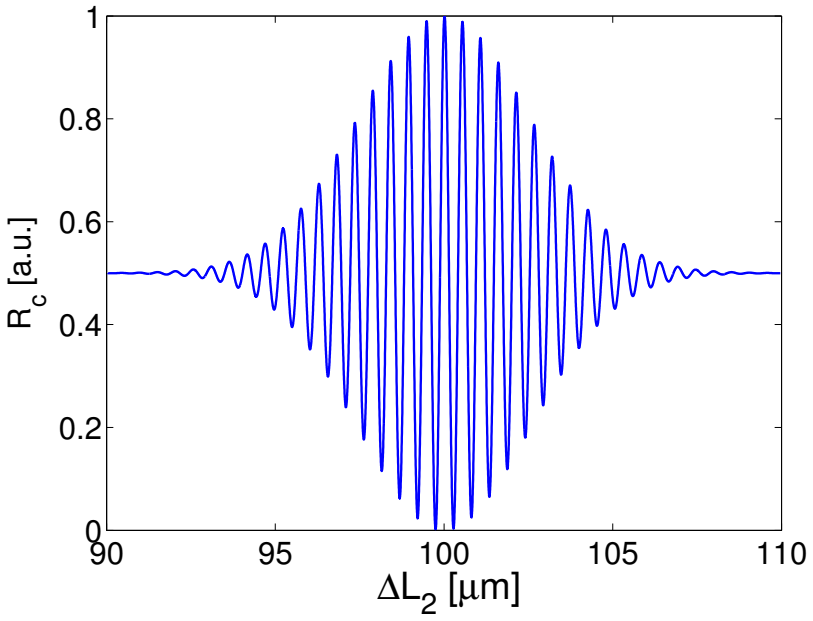

FIG. 6. Coincidence rate of a Franson experiment in a flat spacetime.

C. Second-order correlation function in Schwarzschild coordinates

The experiment presented in Section VII A is now modified as depicted in Fig. 7: One of the MZIs is kept fixed in Alice's lab on the surface of the Earth with $r_A = r_E$. The arms of the interferometer are taken to be smaller than the curvature scale of the spacetime. The second interferometer is positioned at r_B in Bob's lab, i.e. at the altitude of his satellite, and again with arms shorter than the curvature scale. Coincidences between the detectors D_1 and D_2 are detected by time tagging the individual detections.

In the following we use the photon annihilation operators according to the propagating wavepacket approach of Eq. (47). We can then carry out the calculation as in Section VII B. The annihilation operators at the

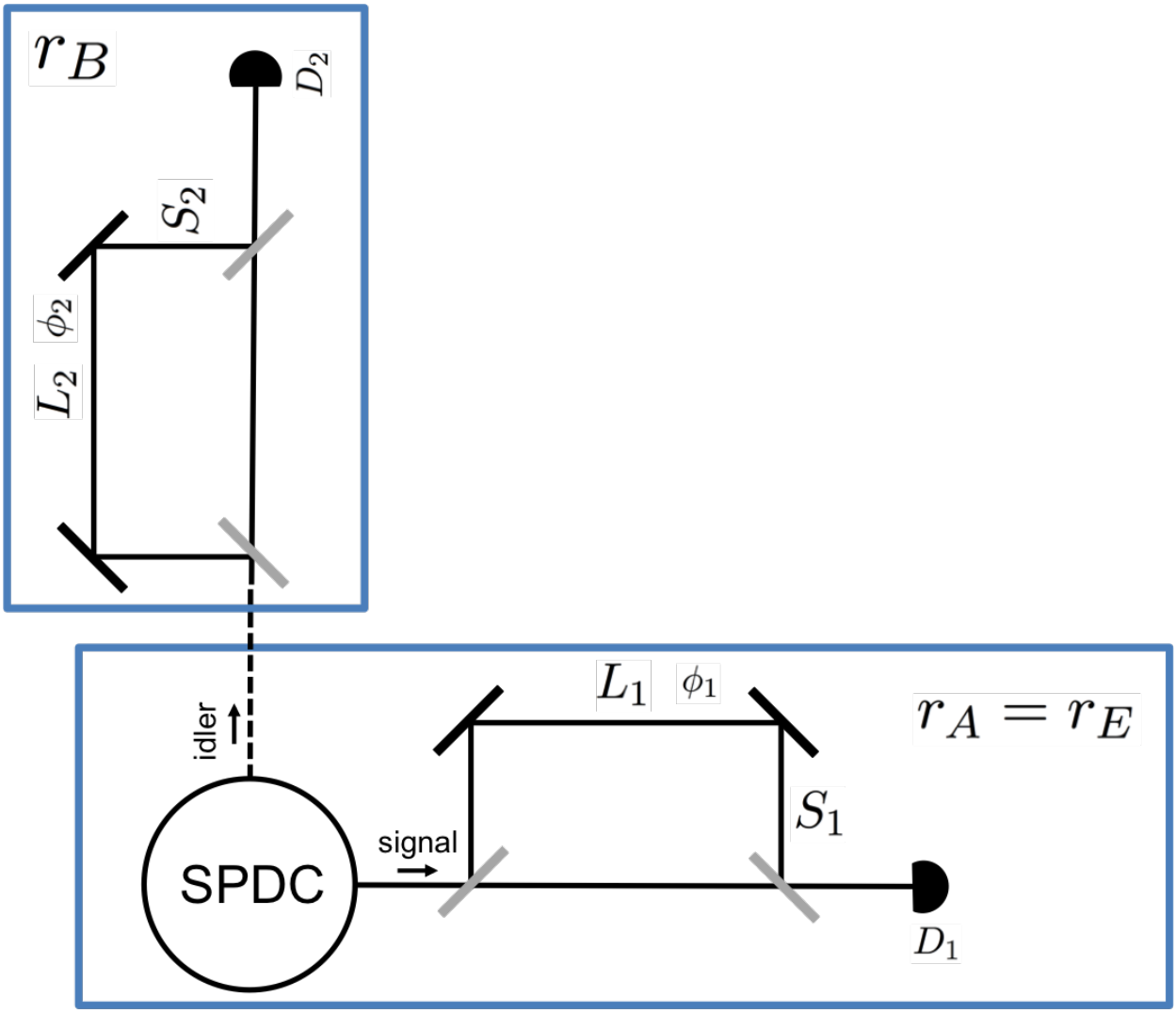

FIG. 7. Modified Franson experiment in a curved spacetime: One of the MZIs is kept fixed in Alice's laboratory on the surface of the Earth while the second interferometer is now placed on Bob's satellite. We denote by r_A and r_B their respective radial coordinates

position of the detectors D_1 and D_2 are now given by

$$a_1(x_A, S_1, L_1, t_1) = \frac{1}{2} a_s(x_A, S_1, t_1) + \frac{1}{2} \mathrm{e}^{i\phi_1} a_s(x_A, L_1, t_1) \tag{120}$$
$$= \frac{1}{2} \int d\omega_s \, F_{\omega_0}(\omega_s) \mathrm{e}^{i\omega_s(x_A+S_1)-i\omega_s t_1} a_{\omega_s} + \frac{1}{2} \mathrm{e}^{i\phi_1} \int d\omega_s \, F_{\omega_0}(\omega_s) \mathrm{e}^{i\omega_s(x_A+L_1)-i\omega_s t_1} a_{\omega_s} \, ,$$

and

$$a_2(x_B, S_2, L_2, t_2) = \frac{1}{2} a_i(x_B, S_2, t_2) + \frac{1}{2} \mathrm{e}^{i\phi_2} a_i(x_B, L_2, t_2) \tag{121}$$
$$= \frac{1}{2} \int d\omega_i \, F_{\omega_0}(\omega_i) \mathrm{e}^{i\omega_i(x_B+S_2)-i\omega_i t_2} a_{\omega_i} + \frac{1}{2} \mathrm{e}^{i\phi_2} \int d\omega_i \, F_{\omega_0}(\omega_i) \mathrm{e}^{i\omega_i(x_B+L_2)-i\omega_i t_2} a_{\omega_i} \, .$$

Apart from the spectral distribution and the linear phase for the radial position of Alice and Bob, i.e. x_A and x_B, the operators have the same form as their flat spacetime counterparts Eq. (102) and Eq. (103). For simplicity we assume in the following the detection bandwidths to be infinite, i.e. $F_{\omega_0}(\omega) = 1$ for D_1 and D_2. The formal expression of the second-order correlation function and the corresponding coincidence rate do not change in the framework of a curved spacetime, i.e. we still consider

$$\begin{aligned} G^{(2)}(x_A, S_1, L_1, t_1; x_B, S_2, L_2, t_2) &= \langle \Psi_2 | a_1^\dagger a_2^\dagger a_2 a_1 \, | \Psi_2 \rangle \\ &= |\psi_2(x_A, S_1, L_1, t_1; x_B, S_2, L_2, t_2)|^2 \, . \end{aligned} \tag{122}$$

Using the operators of Eq. (120) and Eq. (121) we obtain for the coincidence rate

$$R_c \propto \frac{1}{T_c} \int_0^{Tc} dt_1 \int_0^{Tc} dt_2 \, G^{(2)}(x_A, S_1, L_1, t_1; x_B, S_2, L_2, t_2) \, . \tag{123}$$

We again consider a type-II entangled two-photon state in the CW approximation given by

$$|\Psi_2\rangle = \int d\omega \, \Phi(\omega, \omega_{cp} - \omega) \, |1_\omega\rangle |1_{\omega_{cp}-\omega}\rangle \, . \tag{124}$$

Note that the additional phase $\mathrm{e}^{ix_A(\omega_s+\omega_i)}$ taking into account the radial position of Alice, who owns the source, cancels as soon as we assume a distribution for the CW pump field of $\delta(\omega_s + \omega_i - \omega_{cp})$. With the same procedure outlined in Section VII B we obtain

$$\lim_{T_c \to \infty} \left(\frac{1}{T_c} \int_0^{T_c} dt_1 \int_0^{T_c} dt_2 \, |\psi(x_A, X_1, t_1; x_B, X_2, t_2)|^2 \right) = \pi \int d\omega \, |\Phi(\omega)|^2 = \pi \, , \tag{125}$$

in the limit of $T_c \gg \tau_{s,i}^{coh}$ where we used Eq. (109). Again we denote $X \in \{S, L\}$. The first non-constant term in Eq. (107) now generates the additional phases in x_A and x_B and is calculated to be

$$\begin{aligned} A_1 &= \mathrm{e}^{i(\phi_1+\phi_2)} \frac{1}{T_c} \int_0^{T_c} dt_1 \int_0^{T_c} dt_2 \, \psi(x_A, L_1, t_1; x_B, L_2, t_2) \psi^*(x_A, S_1, t_1; x_B, S_2, t_2) \\ &= \mathrm{e}^{i(\phi_1+\phi_2)} \mathrm{e}^{i\omega_{cp}(L_2-S_2)} \frac{1}{T_c} \int_0^{T_c} dt_1 \int_0^{T_c} dt_2 \left[\int d\omega \, \Phi(\omega) \mathrm{e}^{i\omega\{(x_A-x_B)+(L_1-L_2)\}} \mathrm{e}^{-i\omega(t_1-t_2)} \right] \\ &\times \left[\int d\omega' \, \Phi^*(\omega') \mathrm{e}^{-i\omega'\{(x_A-x_B)+(S_1-S_2)\}} \mathrm{e}^{i\omega'(t_1-t_2)} \right] \, . \end{aligned} \tag{126}$$

Commuting the t and ω integrals and using Eqs. (112, 113, 114) we find

$$A_1 = \pi \mathrm{e}^{i(\phi_1+\phi_2)} \mathrm{e}^{i\omega_{cp}(L_2-S_2)} \int d\omega \, |\Phi(\omega)|^2 \mathrm{e}^{i\omega(\Delta L_1 - \Delta L_2)} \, . \tag{127}$$

Note that this is the same expression for A_1 as obtained in the flat space case since the information about the radial coordinates x_A and x_B cancels due to the integration over the detection times which results in a $\delta(\omega - \omega')$ function. (We set here $c = 1$.) We again obtain for the coincidence rate

$$R_c \propto \frac{1}{2} \left[1 + Re \left\{ V(\Delta L_1, \Delta L_2) \mathrm{e}^{i(\phi_1+\phi_2)} \mathrm{e}^{i\omega_{cp}\Delta L_2} \right\} \right] \, , \tag{128}$$

with a visibility given by Eq. (119). We have shown that the arrangement of the Franson experiment according to Fig. 7 leads to the same coincidence rate as in a flat spacetime when expressed in the Schwarzschild coordinates of the asymptotic observer. Note, that in the calculations presented in this Section we explicitly integrated over the detection times t_1 and t_2, i.e. we consider here a time-averaged measurement which will resemble actual experiments, since the coherence time of the entangled photons is up to six order of magnitudes below the timing resolution of the detectors if conventional coincidence electronics is considered. By choosing the detection time window large enough, in fact we considered $T_c \to \infty$, we implicitly took into account the time of flight delay of the idler photon propagating to the detector of Bob. Thus the phase in $(x_A - x_B)$ does not play any role in the final result. No further effects of the curved spacetime background are left.

As in the previous Sections we can express the result obtained by the asymptotic observer in the local frame of Alice or Bob. To do so we use the invariant $\omega_{cp}\Delta t_2 = \Omega_{cp}\Delta\tau_B$ and, according to Eq. (4), $\Delta\tau_A = N_{OA}\Delta L_1$ and $\Delta\tau_B = N_{OB}\Delta L_2$. Further, we use the transformation

$$\Phi^A(\Omega_A) = \sqrt{N_{OA}}\Phi(N_{OA}\Omega_A)\,, \tag{129}$$

in analogy to Eq (46), to rewrite the rate of Eq. (128) in the local frames of Alice and Bob

$$R_c \propto \frac{1}{2}\left[1 + Re\left\{\mathrm{e}^{i(\phi_1+\phi_2)}\mathrm{e}^{i\Omega_{cp}\Delta\tau_B}\int d\Omega_A\,|\Phi^A(\Omega_A)|^2\mathrm{e}^{i\Omega_A\left(\Delta\tau_A - \frac{N_{BO}}{N_{AO}}\Delta\tau_B\right)}\right\}\right]\,, \tag{130}$$

using the fact that ΔL_1 and ΔL_2 are time differences in the asymptotic frame when divided by c. Note further that Ω_{cp} is now expressed in the local frame of Bob according to $\Omega_{cp} = N_{BO}\omega_{cp}$. Equation (130) is to be interpreted as follows: Once Alice has fixed the arm lengths of her interferometer and thus $\Delta\tau_A$, Bob will measure R_c as a function of the arm length difference, i.e. $\Delta\tau_B$, in his reference frame. To evaluate Eq. (130) Bob needs to additionally know $\Delta\tau_A$ and the spectral distribution $|\Phi^A(\Omega)|^2$ from Alice.

1. The Franson experiment and the CHSH Bell-inequality

The maximal visibility observed in the interference fringes of a Franson experiment can be related to the violation of a Bell-inequality [32–34], here the Clauser-Horne-Shimony-Holt (CHSH) inequality [35], and thus, to the entanglement content of the state under study. In the limit of an infinitely small NLC, i.e. $L \to 0$, and the CW pump field approximation, the rate of Eq. (128) can be related to the rate obtained by probing a maximally entangled 2-qubit state

$$|\psi\rangle^{(2)} = \frac{1}{\sqrt{2}}\left(|0\rangle_s|0\rangle_i + |1\rangle_s|1\rangle_i\right)\,. \tag{131}$$

Here, we associate $|0\rangle_{s,i}$ with the short and $|1\rangle_{s,i}$ with the long interferometer paths. More generally, we assume that the above 2-qubit state is described by by a symmetric noise model

$$\rho^{(2)} = \lambda|\psi\rangle^{(2)\,(2)}\langle\psi| + (1-\lambda)\mathbb{1}_4/4\,, \tag{132}$$

where deviations from a pure state are quantified by λ and $\mathbb{1}_4$ denotes the 4-dimensional identity operator. Here, we are particularly interested in deviations from a pure state due to the propagation of the photon through a curved spacetime, the latter potentially inducing some decoherence effects reducing the entanglement of the state. It can be shown that the parameter λ can be related to the violation of a Bell-inequality according to

$$I(\rho^{(2)}) = \lambda I^{max}\,, \tag{133}$$

where I^{max} denotes the value of the maximal violation of the CHSH inequality. In general this inequality is violated for $I(\rho^{(2)}) > 2$. Consequently there exists a critical $\lambda^c \doteq 2/I^{max}$ where for all $\lambda > \lambda^c$ we have a violation of the CHSH inequality. It can be shown that the parameter λ can be related to the visibility of interference fringes [33] and thus we we obtain a critical visibility $V^c \doteq V(\lambda_c)$ above which the CHSH inequality is violated. Explicitly, for the here considered Bell scenario we have $V^c = 1/\sqrt{2}$. Equation (128) shows the same result as in a flat spacetime having a maximal visibility of one (Fig. 6) in the coincidence rate. This implies $\lambda = 1$ and we still have a maximally entangled state although one of the two photons propagated through a curved spacetime from Alice to Bob. Consequently, the Franson scenario sketched in Fig. (7) leads to a maximal CHSH violation. This finding is consistent with the outcomes of the previous Sections namely that standard QFTCS does not show any degradation in entanglement due to a curvature of spacetime. Therefore, it would be interesting to consider the Franson experiment scenario within alternative theories, as for instance provided by the event operator formalism [15, 36], to investigate if a decrease in the violation of a CHSH Bell-inequality and thus a reduction of entanglement in the state appears in a non-standard QFTCS approach.

2. The Franson experiment as a redshift detecting experiment

Again, as outlined in Section VI B (Fidelity), the Franson experiment can be used to detect deviations from a flat spacetime through redshift based effects. In particular, Bob could calculate the expected coincidence rate if a flat spacetime is assumed, which corresponds to the case where $N_{AO} = N_{BO}$, and compare the expected results with the effectively measured rate given by the above equation for $r_B > r_A$, i.e. $N_{BO} < N_{AO}$. The deviation would then be due to the gravitational redshift. To be more quantitative we consider the spectral amplitude function of Eq. (129) in a normalized Gaussian form according to

$$\Phi^A(\Omega_A) = \sqrt{\frac{N_{OA}}{\Delta\omega_{s,i}\sqrt{\pi}}}\, \mathrm{e}^{-\frac{(N_{OA}\Omega_A)^2}{2\Delta\omega_{s,i}^2}}, \tag{134}$$

where Ω_A is a relative frequency. For the width of the entangled photon spectra we consider in the following a typical bandwidth of 100 nm which corresponds to $\Delta\omega_{s,i} = 166.4\,\mathrm{THz}$. We further fix $\Delta\tau_A$ in Eq. (130) by choosing $\Delta L_1 = 100\,\mu\mathrm{m}$. A deviation in the count rate due to the redshift is then characterized by the overlap function

$$\Xi_{R_c} \doteq \frac{\int_{-\infty}^{\infty} d\Delta\tau_B\, R_c(\Delta\tau_B, N_{AO}, N_{AO}) R_c(\Delta\tau_B, N_{AO}, N_{BO})}{\int_{-\infty}^{\infty} d\Delta\tau_B\, R_c(\Delta\tau_B, N_{AO}, N_{AO})^2}, \tag{135}$$

where we define $R_c(\Delta\tau_B, N_{AO}, N_{BO}) \doteq R_c - 1/2$ to confine the integration to a convergent result. As expected for consistency it holds that $\Xi_{R_c} = 1$ for $N_{BO} = N_{AO}$. Figure 8 shows the deviation for $1 - \Xi_{R_c}$ (blue line) as a function of the altitude of Bob with respect to Alice.

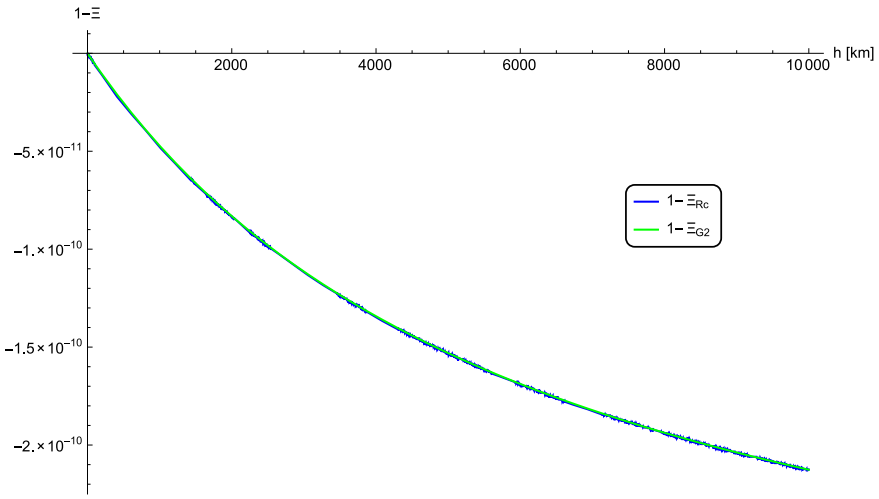

FIG. 8. Redshift deviation according to Eq. (135) and Eq. (136).

The Franson setup, involving two interferometers to be adjusted and synchronized, is, from an experimental point of view, a quite demanding arrangement. One could ask whether a simpler measurement of a second-order correlation function shows sufficient sensitivity to redshift effects to obviate the need for the Franson experiment. To answer this question we define, according to Eq. (135) the overlap function

$$\Xi_{G^{(2)}} \doteq \frac{\int_{-\infty}^{\infty} d\tau_B\, G^{(2)}(\tau_B, N_{AO}, N_{AO}) G^{(2)}(\tau_B, N_{AO}, N_{BO})}{\int_{-\infty}^{\infty} d\tau_B\, G^{(2)}(\tau_B, N_{AO}, N_{AO})^2}, \tag{136}$$

where $G^{(2)}$ is determined by

$$\psi^{(2)}(\tau_B, N_{AO}, N_{BO}) \doteq \int d\Omega_A \, \Phi^A(\Omega_A) \mathrm{e}^{i\Omega_A\left(\tau_A - \frac{N_{BO}}{N_{AO}}\tau_B\right)}. \tag{137}$$

Note, that Eq. (137) can be derived by applying the same transformation rules to Eq. (97) as used for Eq. (130) and neglecting the additional propagation phase. We further set $F_{\omega_0} = 1$ and use again Eq. (134) for the spectral amplitude. Here, the time τ_A has a different meaning than $\Delta\tau_A$ in the Franson experiment, where the latter corresponds to the path length difference of Alice's interferometer. For the second-order correlation function, Alice sends the photon at time τ_A with respect to her reference frame; as this is arbitrary we, without loss of generality, set $\tau_A = 0$ in what follows. The detection then occurs at time τ_B in Bob's frame, or the rescaled time $\frac{N_{BO}}{N_{AO}}\tau_B$ if we express it in Alice's frame - this is due to redshift effects. We additionally depict $1 - \Xi_{G^{(2)}}$ in Fig. 8 (green line). As can be seen, the sensitivity for redshift detection in the Franson experiment is equal to a second-order correlation experiment. No particular advantage is gained due to the oscillatory behaviour in the Franson signal.

VIII. Experimental implementation

A. Introduction

Beside testing the interplay between quantum mechanics and general relativity, entangled photon pairs are also a key resource for optical quantum communication, which involves the transmission of quantum states of light, such as squeezed states, single photons or entangled photons. Here we consider the specific, but relevant, scenario shown in Fig. 2. Entangled photon pairs are generated at a certain location, one of the photons being locally detected (Alice), while the other photon is transmitted through a free-space optical link to a remote detection (Bob). One of the constraints of transmitting quantum states over large distances is the low link transmission T due to the combined effects of beam diffraction, transmission through the atmospheric, and pointing requirements [37]. This limits the rate of quantum communication. It is thus of interest to generate and detect entangled pairs at the highest possible rate. Moreoever, when testing standard QFTCS, novel effects are expected to be small in the vicinity of the Earth, such that large statistics will have to be acquired for a deviation to be detected, requiring again high generation and detection rates.

B. Evaluation of signal to noise ratio

To illustrate the relevance of the detection rate, we evaluate the signal to noise ratio as a function of the detection rate and detector noise. The coincidence rate R_{coinc} in the experiment depicted in Fig. 2 is given

by

$$R_{coinc} = TR_{det}, \tag{138}$$

where T includes both the transmission of the channel and the detection efficiency of the associated detector and R_{det} is the single count rate at Alice. False coincidences R_{acc}, also called accidental coincidences or accidentals, are here mainly due to coincidences between detected photons on Alice's side and dark counts on Bob's side, i.e.

$$R_{acc} = R_{det}R_{dc}\Delta t_{coinc}, \tag{139}$$

where R_{dc} is the dark count rate of the detector and Δt_{coinc} the length of the coincidence window (in the following, it is taken to be optimal, i.e. equal to the temporal resolution of the detector).

The signal of interest S can be, for instance, the differences in the expected count rates between the predictions of two different theories. At first approximation, it is proportional (and usually small) to the coincidence rate $S = \epsilon R_{coinc}$. This signal has to be distinguished from the noise, which we here assume to be shot noise limited $N = \sqrt{R_{coinc} + R_{acc}}$, such that the signal to noise ratio for 1 s measurement time is given by

$$\frac{S}{N}(1s) = \epsilon\sqrt{R_{det}}\frac{T}{\sqrt{T + R_{dc}\Delta t_{det}}}. \tag{140}$$

The signal to noise ratio after an integration time of t is then

$$\frac{S}{N}(t) = \frac{S}{N}(1s)\sqrt{t} \tag{141}$$

and the time needed to achieve a signal to noise ratio of 1 is

$$t_{S/N=1} = \frac{T + R_{dc}\Delta t_{det}}{R_{det}T^2\epsilon^2}. \tag{142}$$

Figure 9 shows this time as a function of the parameter ϵ for typical values $R_{dc} = 10$Hz, $\Delta t_{det} = 100$ps and $T = 3 \times 10^{-4}$ [38], and for $R_{det} = 1$MHz and $R_{det} = 1$GHz. It illustrates the need of large count rate at Alice. With standard detectors saturating around 1 MHz the smallest value of ϵ which could be detected in 1 day (10^5 s) of acquisition is of the order of 2×10^{-4}. By multiplexing the detectors as we will see in the following, 1 GHz count rate could be feasible, such that the smallest ϵ could be $\sqrt{1000}$ times smaller, about 6×10^{-6}.

The actual value of ϵ is dependent on the experiment to be performed and on the theory to be tested. For instance, if one aims at testing only general relativitic effects with entangled photons (or single photons), ϵ will be on the order of 10^{-10}. The event operator theory [15, 36], on the other hand, predicts much larger deviations from flat space, with i. e. $\epsilon \approx 0.5$.

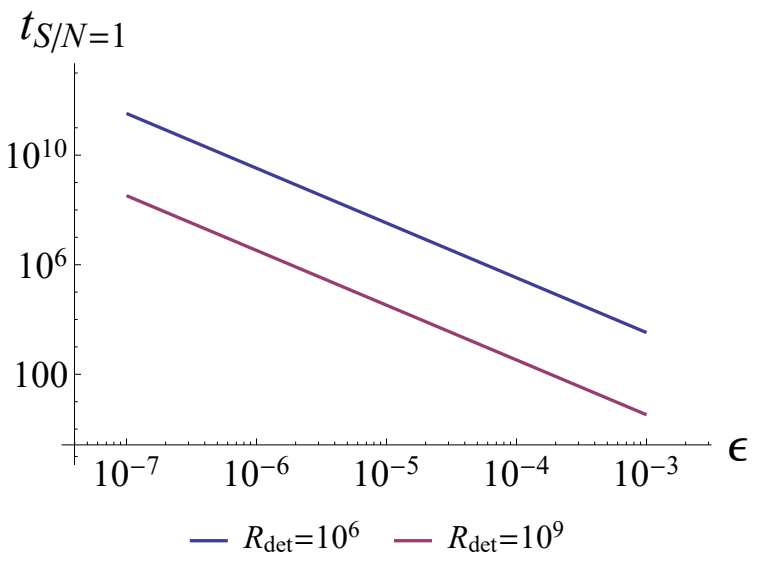

FIG. 9. Time needed to achieve $S/N = 1$ as a function of the parameter to measure ϵ, for a count rate of 10^6 and 10^9

C. Sources of entangled photons

Before evaluating the detectors we introduce a common way to generate entangled photon pairs through spontaneous parametric down conversion (SPDC) in a non-linear crystal (NLC) [27]. This process appears when a NLC is pumped by a laser beam strong enough to induce a second-order susceptibility $\chi^{(2)}$ process. In this case, a pump photon (p) may be annihilated and two new photons of lower frequencies, the signal(s) and idler (i), are created. SPDC is governed by energy conservation

$$\omega_p = \omega_s + \omega_i, \tag{143}$$

where ω_j denotes the angular frequency with $j \in \{p, s, i, \}$ of the involved photons, transverse momentum conservation

$$\mathbf{q}_p = \mathbf{q}_s + \mathbf{q}_i, \tag{144}$$

and momentum conservation in z-direction (given by the pump beam)

$$k_{pz} = k_{sz} + k_{iz} - \Delta k_z. \tag{145}$$

Here, Δk_z denotes a possible momentum mismatch in the z-direction which governs the efficiency of the SPDC process such that, for all $\Delta k_z \neq 0$, the efficiency of SPDC gets reduced. In what follows we restrict the propagation direction of the two down-converted photons to be collinear with the pump photon, i.e. $\mathbf{q}_s = \mathbf{q}_i = \mathbf{0}$. We further constrain the derivation of the entangled two-photon state to the case where the

signal and idler photons are extraordinarily (e) and ordinarily (o) polarized; this configuration is referred to as type-II SPDC [39–44] and allows to deterministically separate the two photons by means of a polarizing beam splitter (PBS) after the NLC, which is a common procedure to guide the signal and idler to separated detection units. Type-II SPDC leads to a variety of emission patterns of the down-converted photons. Exact calculations of these patterns can be found in [39]. We rely here on the graphical representations in Fig. (10) and Fig. (11) both taken from [41].

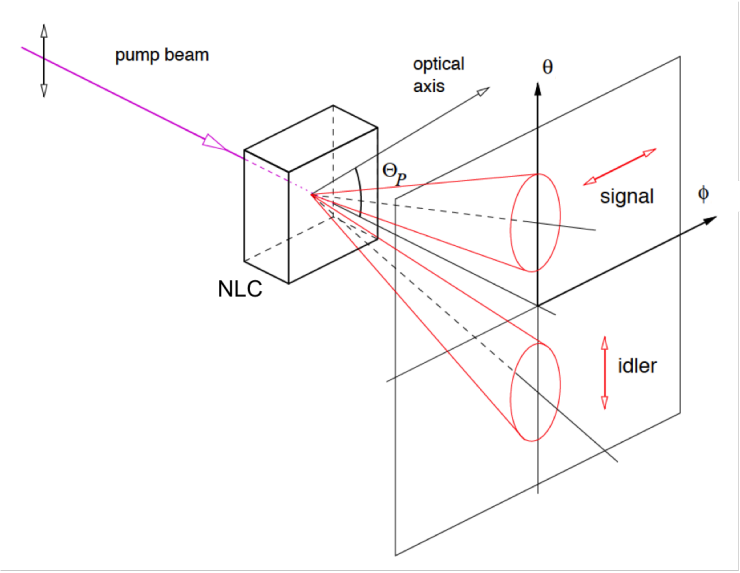

FIG. 10. Geometrical arrangement for type-II spontaneous parametric down-conversion. [41]

Figure (10) shows a geometrical representation of type-II SPDC. A collimated pump beam enters a NLC. The down-converted photons are emitted in two cones where the cone of the signal is e (horizontally) and the cone of the idler is o (vertically) polarized. The shape and the overlap of the two cones can be altered by varying the angle Θ_p between the propagation direction of the pump and the optical axis of the NLC. This is shown in Fig. (11) where $\Delta\Theta = \Theta_p + \Theta_0$ is the angle between the pump direction and the normal of the end face of the NLC (Θ_0 is the angle between the NLC face and its optical axis). In the here proposed experiments we consider the case where $\Delta\Theta = 0°$ which implies a single point of intersection at $\Theta = \phi = 0°$ of the two cones (see Fig. (10)). At this particular point a collinear distribution of the involved photons is realized. Moreover, it can be shown that at this point the signal and idler photon have the same center frequency which is related to the frequency of the pump photon according to $\omega_{cs} = \omega_{ci} = \omega_{cp}/2$ (no matter whether the pump laser is pulsed or continuous wave) [39, 42]. This is referred to as the frequency degenerated case of SPDC. Experimentally, the corresponding state is selected by placing a pinhole at $\Theta = \phi = 0°$.

To calculate the corresponding two-photon state we start with the interaction Hamiltonian for type-II SPDC

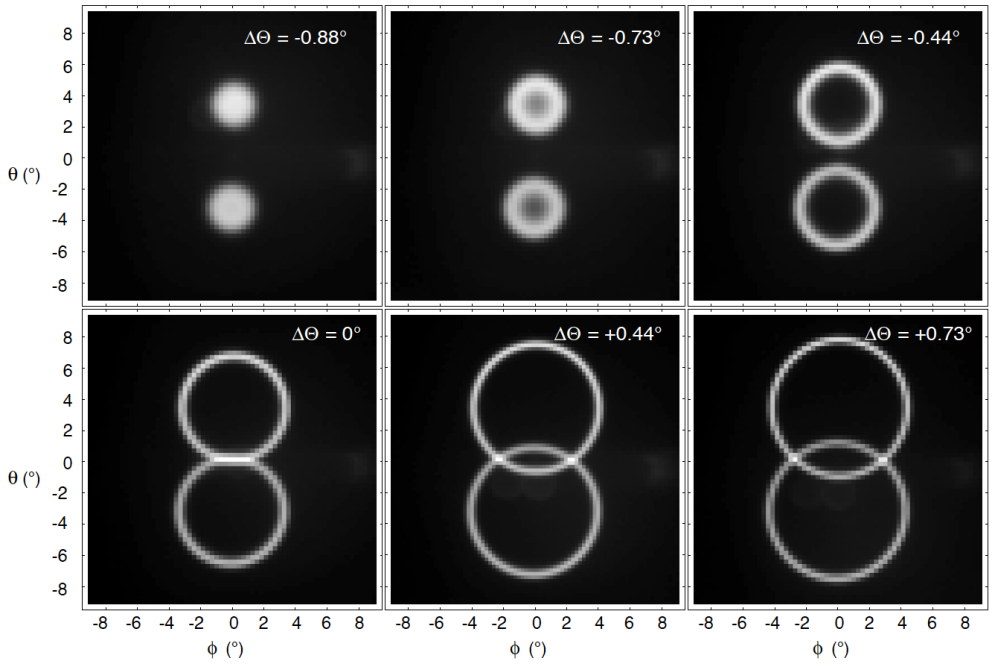

FIG. 11. Measured angular distribution of the down-converted light for different NLC orientations. For $\Delta\Theta = 0^\circ$ the incidence direction of the pump field coincides with the normal of the crystal face. For the specific point of overlap between the two cones this corresponds to the situation where the pump, the signal, and the idler propagate collinearly [41].

given by

$$\hat{H}_{int}(t) = \varepsilon_0 \int_V d^3r\ \chi^{(2)}(z)\ \hat{E}_s^-(z,t)\hat{E}_i^-(z,t)E_p^+(z,t) + \text{H. c.}, \tag{146}$$

where ε_0 denotes the electric permittivity of the vacuum and $\chi^{(2)}(z)$ is the nonlinear susceptibility which governs the strength of interaction between the three fields.[3] We assume here $\chi^{(2)}(z)$ as frequency independent since we assume the SPDC process is far away from any resonance frequency of the non-linear material. Due to the strong intensity of the pump laser we treat the associated field as a classical quantity whereas the signal and idler photons are expressed as their corresponding operators according to Eq. (32) for $H = 1$ and restricted to the longitudinal direction. Since SPDC is a weak interaction process in bulk crystals, it is sufficiently accurate to calculate the corresponding two-photon state by means of time-dependent perturbation theory up to first-order in the interaction picture. This implies

$$|\Psi_2(t)\rangle = |0\rangle - \frac{i}{\hbar}\int_{t_0}^{t} dt'\ \hat{H}_{int}(t')|0\rangle, \tag{147}$$

where we consider the state at the initial time t_0 to be the composite vacuum state $|0\rangle \doteq |0\rangle_i|0\rangle_s$. The integration over t' is evaluated under the approximation that the interaction of the involved photons proceeds

[3] We use here hats on operators to distinguish them from c-numbers.

adiabatically within a finite region of time [27]. The integration boundaries can thus be extended according to $t_0 \to -\infty$ and $t \to +\infty$ which imposes strict energy conservation. As a result, $|\Psi_2(t)\rangle$ becomes time independent. The state is then calculated by inserting the explicit expressions for the pump field and the field operators in $\hat{H}_{int}$, so that the final type-II entangled two-photon state reads

$$|\Psi_2\rangle = |0\rangle + \int_0^\infty d\omega_s \int_0^\infty d\omega_i \; \Lambda(\omega_s, \omega_i) \; a^\dagger_{\omega_s} a^\dagger_{\omega_i} |0\rangle. \tag{148}$$

The function $\Lambda(\omega_s, \omega_i)$ is referred to as the joint-spectral amplitude (JSA).[4] The state of Eq. (148) is entangled since the JSA can in general *not* be written as $\Lambda(\omega_s, \omega_i) = g(\omega_s)h(\omega_i)$. Note, that the index s and i differentiates here the photons with regard to their distinguished polarization degree of freedom. (We have associated the signal photon with extraordinary and the idler photon with ordinary polarization.) Accordingly, the commutation relations are given by Eq. (72). In the following we consider the SPDC process stimulated by a continuous wave (CW) laser. The JSA then reads

$$\Lambda(\omega_s, \omega_i) \propto \delta(\omega_{cp} - \omega_s - \omega_i) \int_{-L}^{0} dz \, \chi^{(2)}(z) \mathrm{e}^{i\Delta k_z z}, \tag{149}$$

where L is the length of the NLC and the longitudinal momentum mismatch is explicitly given by

$$\Delta k_z \doteq k_p(\omega_s + \omega_i) - k_s(\omega_s) - k_i(\omega_i). \tag{150}$$

For convenience we define the phase-matching function

$$\Phi(\omega_s, \omega_i) \doteq \int_{-L}^{0} dz \, \chi^{(2)}(z) \mathrm{e}^{i\Delta k_z . z}. \tag{151}$$

(See also Eq. (2) in [45]). The wave vectors $k_j = n_j(\omega_j)\omega_j/c$, $(j = p, s, i)$, depend on the extraordinary and ordinary refractive indices n_j. The efficiency of the SPDC process is reduced by the walk-off between the involved fields due to the birefringence of the NLC. In order to compensate for the walk-off effects and therefore to minimize Δk_z a technique called quasi-phase matching (QPM) is used. This involves NLCs with a specific poling of the optical axis adjusted to the needs of the experiment. The structure of the poling finally determines the functional dependence of $\chi^{(2)}(z)$ and thus the JSA [45, 46]. The JSA finally determines the coherence time $\tau^{coh}_{s,i}$ of the photons. Using specific aperiodic, i.e. chirped, poling schemes, ultra-narrow coherence times down to 7 fs have been observed in a Hong-Ou-Mandel measurement [47].
As seen from Eq. (146), the emission rate is proportional to the power of the pump laser which can, in principle, be arbitrary large. High emission rates can be achieved in standard poled crystals with a few Watts of laser power [34]. The fundamental limit is not the pump power but the fact that the pair emission

[4] To be consistent with the notation of the previous chapters we shall drop the hats on the operators.

process is random. This is why, in order to stay in the single pair regime, where the first order perturbation of the interaction is valid, and avoid the emission of multiple pairs at the same time, the mean number of pairs per mode $\bar{n}$ should be kept small, usually below 0.1. For pulsed operation, this means that the mean number of emitted pairs per pulse should be below 0.1. With GHz ultrashort fs lasers available, GHz pair emission rate could be achieved. In the continuous regime, $\bar{n}$ is given by $\tau_{s,i}^{coh}/\tau_{SPDC}$ with τ_{SPDC} being the mean time between two pairs. In term of bandwidth, we can express this as $\bar{n} = R_{SPDC}/\Delta\omega_{s,i}$ with R_{SPDC} the pair emission rate and $\Delta\omega_{s,i}$ the spectral width of the emitted photons. With broadband emission of several tens of nm [34], $\Delta\omega_{s,i}$ can be as large as 10 THz, thus allowing in principle rates in the THz regime, still being in the single pair regime. Such large emission rates have been realized experimentally but only observed by low efficiency optical coincidence scheme [48].

Unfortunately, the present single photon counters do not sustain such high rates. Their limit depends of the particular technologies. For single pixel detectors (not multiplexed) the best performances are achieved by superconducting nanowire single photon detectors (SNSPDs). Here, commercial detectors with more than 50 MHz count rates are available (www.singlequantum.com), while silicium avalanche photodiodes saturate at about 10 MHz (www.micro-photon-devices.com). It is thus clear that the limiting factor for high rates is not the source but the maximal achievable counting rate of the single photon detectors; and this in both regimes, pulsed or continuous.

D. Model of detectors

Ultimately, the maximal rate is limited by the temporal resolution of the detector, as one should be able to uniquely assign a detection time to each detected photon. However the detectors are usually limited by their dead time which is much larger than the temporal resolution. The general way to overcome the dead time of a single detector is to multiplex several of them [49]. This can be achieved by splitting the photon flux either with cascaded fiber beamplitters or by illuminating an array of detectors with a wide beam.

For coincidence detection between remote events, it is necessary to be able to time stamp each detection event. This, together with the requirement of a very high detection rate, means that the performance of the system will be affected by the dead time, timing jitter, efficiencies and dark count rate of the individual detectors. Moreover, for a large number of multiplexed detectors, further constraints will appear. In particular the data rate (bandwidth) of the readout system can be very high, namely from the sensor to its memory and further to the acquisition system. In addition, integrating detectors and electronics on the same chip have detrimental effects on the effective efficiency (reduced fill factor). In the following we first estimate the performance of an ideal scheme for the multiplexing of detectors. Then we show, based on experimental

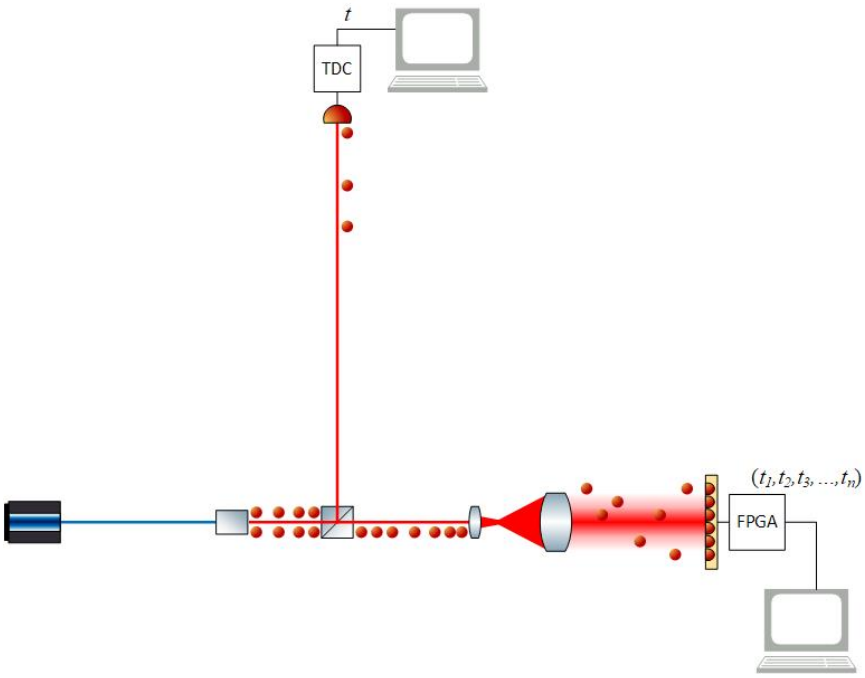

FIG. 12. Scheme of the coincidence detection setup with multiplexed detctors.

results of CMOS technology, where the actual bottlenecks are and propose some strategies to overcome them.

Figure 12 shows the investigated scheme making use of a multiplexed detection in continuous mode. As previously, a NLC emits an intense flux of photon pairs in a stochastic way with a rate of R_{SPDC}. One photon of a pair is send through a channel of transmission T to Bob's detector, which doesn't need to sustain a high counting rate, but requires a high temporal resolution in the time tagging of the detection events. The other photon is locally detected by a high rate detector at Alice. We are interested in maximizing the coincidence rate of detection, by maximizing the number of detected pairs.

1. Ideal continuous operation

At first we investigate the case of an ideal multiplexed detector, where its limits are only given by the limits of the single pixel detectors and where the multiplexing process doesn't introduce any additional constraints. In that case, the maximal count rate, in a scheme of multiplexed slow detectors, is ultimately limited, by the number of single pixels, their dead time and by the temporal resolution of the detectors. The relevant parameters for such detectors are listed in Table I, with typical values for CMOS technology.

With R_{SPDC} impinging photons, the detected count rate is, to a first approximation, given by $R_{det}^{max} = \eta R_{SPDC}$. It is also limited by the two factors already introduced. On the one hand, the dead time of each

TABLE I. Detector parameters in continuous operation

Description	Symbol	Typical value	Unit
Number of pixels	N		
PDE of each pixel	η	0.4	
Dead time of each pixel	t_{dead}	100	ns
Detector resolution	Δt_{det}	100	ps
Dark count rate per pixel	R_{dc}	10	Hz

pixel limits the global count rate to $\frac{N}{t_{dead}}$. On the other hand, there is a global limit to the maximal count rate of $\frac{1}{\Delta t_{TDC}}$, as beyond it is not possible to define more than one single photon detection event per time-bin. Indeed, if such events occur it is no longer possible to assign unambiguously the detected photon to a pair. A simple approximation of the maximal count rate is then

$$R_{det} = \mathrm{Min}\left(\frac{1}{\Delta t_{TDC}}, \frac{N}{t_{dead}}, \eta R_{SPDC}\right). \tag{152}$$

A more detailed description of the saturation should include the Poisson distribution of the detection events [50]. At first, we consider a single pixel detector. Its count rate as a function of efficiency, dead time and impinging flux is given by

$$R_{det} = \frac{R_{det}^{max}}{1 + R_{det}^{max} t_{dead}}. \tag{153}$$

Next, we describe the limitation due to the detector's finite temporal resolution. We make the assumption that the detector has photon number capability detection, such that it can distinguish the events where only one photon was detected from the others, and only keep those single detections as valid detection events. For Poisson distribution, the probability to have one and only one detection within a time window of Δt_{det} is given by $exp(-\lambda)\lambda$ where $\lambda = \eta R_{SPDC} \Delta t_{det}$. The detected count rate is thus

$$R_{det}^{*} = exp(-\eta R_{SPDC} \Delta t_{det}) \eta R_{SPDC}. \tag{154}$$

To take both effects into account, we replace R_{det}^{max} in Eq. (153) by R_{det}^{*} from Eq. (154) such that

$$R_{det} = \frac{exp(-\eta R_{SPDC} \Delta t_{det}) \eta R_{SPDC}}{1 + exp(-\eta R_{SPDC} \Delta t_{det}) \eta R_{SPDC} t_{dead}} = \frac{\eta R_{SPDC}}{exp(\eta R_{SPDC} \Delta t_{det}) + \eta R_{SPDC} t_{dead}}. \tag{155}$$

Figure 13 shows the detected count rate as a function of the impinging count rate for a single pixel detector with the typical value of table I. One can observe three regimes. First a linear dependency between count rate and illumination, then a saturation at a rate given by $1/t_{dead}$ and finally a decrease due to increasing multiple detections.

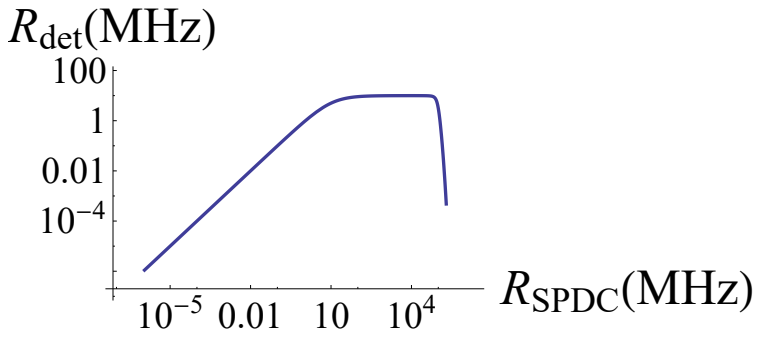

FIG. 13. Detected count rate as a function of R_{SPDC} for a single pixel detector

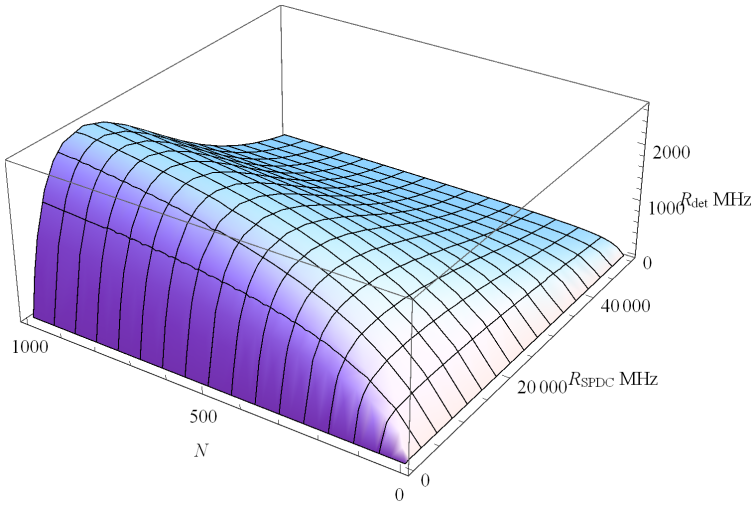

FIG. 14. Detected count rate as a function of R_{SPDC} and N for a multiplexed detector

By multiplexing N pixels one can increase the saturation plateau. The multiplexing is formally described by noting that the illumination on each pixel is reduced by a factor N, when all pixels are uniformly illuminated and, assuming the readout to be perfect, all pixels can be read independently. Therefore the count rate is given by reducing t_{dead} by a factor N, without however changing Δt_{det} which is a global property of the sensor.

$$R_{det}^{N} = \frac{\eta R_{SPDC}}{exp(\eta R_{SPDC}\Delta t_{det}) + \eta R_{SPDC} t_{dead}/N}. \tag{156}$$

Figure 14 shows the detected count rate as a function of the illumination and of the number of detectors. As expected the plateau rises with increasing number of detectors. It is revealing to study the maximum count rate (the height of the plateau) as a function of the number of detectors. It is shown on Fig. 15. One observes a saturation due to the finite temporal resolution of the sensor, occurring at a count rate on the order of $1/\Delta t_{det}$. This is why, with typical values of t_{dead} and Δt_{det}, GHz count rates can be achieved with

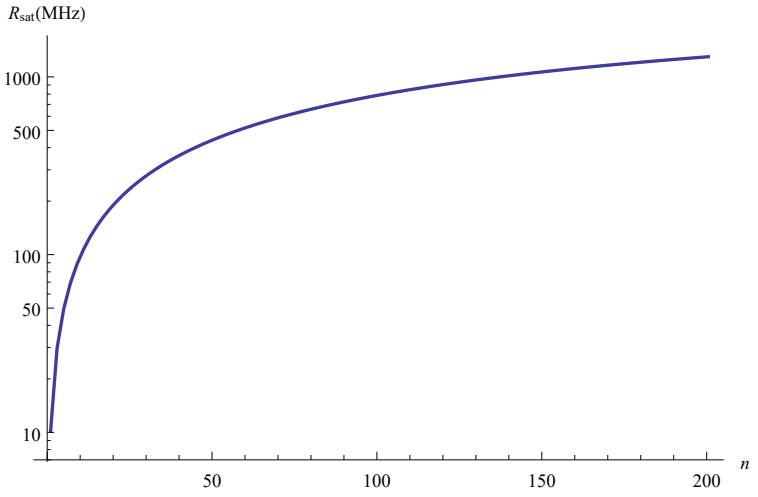

FIG. 15. Saturation level as a function of the number of pixels.

a few hundred pixels. Therefore there is no need for the multiplexing of more than 1000 pixels. Higher count rates could only be achieved by improving the temporal resolution.

Finally we can estimate the data rate in bits/s as

$$R_{data} = -\log_2(\Delta t_{TDC}) R_{det}, \tag{157}$$

where the temporal tagging of the event is uniquely defined modulo 1 s. For a typical temporal size of time bins of 100 ps we need about $\log_2(10^{10}) \approx 32$ bits per detection event, leading to a tremendously large amount of data for large detection rate (4 GB/s for 1 GHz count rate). While than the storage and further processing of those data could be in principle handled with enough processing power, the strong bottleneck is the acquisition of the events recorded on the sensor and their transfer into a memory. A high rate of triggering single photon counters would lead to a high power consumption and to heating of the sensor.

2. *Frame based synchronous detection*

Because a continuous operation is technologically difficult to implement. The current sensors with per pixel temporal resolution are mostly based on a framed based acquisition scheme. Here the detector is active during a temporal frame of length t_{frame} as illustrated on Fig. 16. Within each frame all detection events are time stamped. The readout of the time stamps and their acquisition is performed after the frame and take a given time t_{data}. After a reset time t_{reset} the detector is brought back to its initial state and is ready for the acquisition of a new frame. We have therefore $R_{frame} = \frac{1}{t_{frame}+t_{read}}$ and $t_{read} = t_{data} + t_{reset}$. This scheme is synchronous and the frames are triggered by an external signal. For a continuous source of entangled photons there are obviously limitations with this kind of detector with a limited duty cycle.

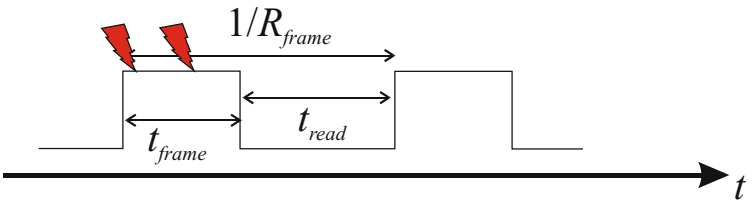

FIG. 16. Active t_{frame} and read t_{read} times of a frame.

As a model, we consider the same detector as before, but with additional parameters given by the frame length and frame rate (Table II).

TABLE II. Detector parameters in continuous operation

Description	Symbol	State of the art	Unit
Number of pixels	N		
PDE of each pixel	η	0.4	
Dead time of each pixel	t_{dead}	100	ns
Detector resolution	Δt_{det}	100	ps
Dark count rate per pixel	DC	10	Hz
Frame rate	R_{frame}	10^5	Hz
Frame length	t_{frame}	50	ns
Fill factor	f	0.2	

In a regime where the effective deadtime t_{dead}/N is smaller than the frame length, the detected signal is then simply given by the expected rate in a continuous operation multiplied by the duty cycle of the detectors

$$R_{det}^{frame} = R_{det}^{cont} \frac{t_{frame}}{t_{frame} + t_{read}} f = R_{det}^{cont} R_{frame} t_{frame} f \ . \tag{158}$$

The duty cycle $R_{frame}t_{frame}$ is, with state of the art parameters, about 5%. In addition the presence on the same chip of sensitive area and electronics, reduces the effective detection area by the so-called fill factor f, thus reducing the effective PDE by the same factor, such that any gain from the multiplexing would be in practice compensated by the low duty cycle. It would be thus of primary relevance to increase both duty cycle and fill factor. In the next section we give more insight to the technological limitations and the solutions to overcome them.

3. Limiting parameters to improve

Table III shows the characteristics of two single photon detector arrays recently developed and used for quantum experiments: SPAD-Net [51] and SuperEllen [52].

TABLE III. Characteristics of sensors

Description	Symbol	SuperEllen	SPAD-Net
Number of pixels	N	1024	128
SPAD efficiency	η	0.05	0.05
SPAD fill factor	f	0.20	0.41
PDE of each pixel	PDE	0.01	0.02
Frame rate	R_{frame}	800 KHz	330 KHz
Frame length	t_{frame}	50 ns	260 ns
Total Readout time	t_{read}	1.25 μ	3 μs
Data Readout time	t_{data}	0.25 μ	2 μ
Reset time	t_{reset}	1 μs	1 μs
TDC resolution	Δt_{TDC}	50ps	65ps
TDC code length	n_{TDC}	256	4096
Pixel deadtime	t_{dead}	100 ns	100 ns
Pixel area	A_{pixel}	2025 μm^2	0.3477mm^2

a. Duty cycle

The duty cycle can be increased by either decreasing the readout time $t_{readout}$ or by increasing t_{frame}. Decreasing the readout time would requires more electrical circuits on the chip. The associated decreasing of the fill factor could be avoided by stacking the electronics on the sensor [53]. Increasing the length of the frame but still keeping the temporal resolution of the detector requires an increase in the depth of time to digital converter (TDC) code; that is, increasing the number of bits of the counter associated to the TDC. For instance 8 bits of TDC code gives a frame length of $2^8 \Delta t_{det}$. Each additional bit takes space on the chip (on the order of 50 μm^2). Consequently the fill factor is reduced by the additional needed space.

b. Fill factor

As mentioned, actual single photon detector arrays are operating in a framed mode because of the need to integrate the time stamping and readout electronics on the chip. A general solution would be stacking. However, for the specific applications discussed here, a micro-lens array on top of the sensor could work efficiently. Indeed, the illumination of the sensor being single mode, the micro-lenses could be designed to couple all light exactly onto the sensitive area of each pixel, thus achieving an effective fill factor close to one.

Another solution is to move the whole time stamping electronics outside of the sensor, as we dont need high spatial resolution for the present application. Such detectors are called Silicon Photo-multipliers (SiPM). They only output one signal, which will have to be time stamped by very fast (GHz) electronics.

c. Operational wavelength

Finally an important parameter for the experimental implementation is the wavelength of the entangled photons. It has to match the sensitivity peak of the detectors but also the transmission window of the optical link. The wavelengths are constrained by the capability of the entangled photon source. Ideally the locally detected photons have a wavelength between 400 and 500 nm where the detector arrays are the most sensitive and the transmitted photon lie between 500 nm and 1000 nm for a high atmospheric transmission [54]. The two wavelengths are related by Eq. (143). Shorter pump wavelengths are of preference but they are limited by the available lasers and non-linear crystals. For instance a source operating with a 375 nm (laser diode) pump and a PPKTP crystal could produce one photon at 1032 nm and the other at 588 nm. Shorter wavelengths could be reached with solid states lasers and periodically poled lithium tantalate crystals [55].

IX. Discussion

We have investigated the effect of spacetime curvature on radially propagated entangled photons, as measured by two spatially separated, static, observers performing interferometry experiments. In particular, for simplicity, we have focused on the exterior Schwarzschild metric, restricted to 1+1 dimensions as a proxy for the Earth. We then considered a down-conversion process generating time-energy entangled photon pairs that are distributed to the observers through the gravitational gradient. The photons were modelled as a scalar field using standard quantum field theory. Then the interaction between the photons and the spacetime was developed using the formalism of quantum field theory in curved spacetime (QFTCS), which, in the absence of a full theory of quantum gravity, provides a semi-classical framework well suited for calculations in regimes of weak gravity.

We found that no novel effects appear when we propagate quantum states, instead of classical light signals, on a curved spacetime. In particular, the visbility of the two photon interferences in a Franson experiment, a measure of entanglement, is unchanged relative to those calculated on a flat spacetime. Similarly, the fidelity of a communication channel using entangled photons is also unaffected. These results hold when the observers are aware of the spacetime they are in; to a good approximation the near-Earth spacetime is described by the exterior Schwarzschild metric, as has been measured by other tests of gravity. This is because, armed with such knowledge, the two observers essentially share a reference frame (or clock) and the only non-trivial effects occur as a result of different locally measured times. Entanglement, as revealed by two-photon Franson interferometry, is also preserved in a curved spacetime.

On other hand, if the observers assume no knowledge of the spacetime - in effect taking it to be flat -

and develop protocols accordingly, they will see their channels as noisy, with reductions in fidelity and/or interferometric visibility, as also reported in [21]. This can either be viewed operationally as an error to correct, as with satellite navigation systems which need to correct for gravitational redshift effects, or as a means of testing gravity (or both) [56, 57]. The change of the measured signal as compared to the one expected in a flat space time is also present in Franson experiment. Viewed as a test of gravitational redshift the Franson experiment, however, does not show any particular advantage in comparison with a simpler experiment, namely the measurement of a second-order correlation function. Both measurements show the same redshift deviation.

The result also changes if one assumes that the correct formalism unifying gravity and quantum mechanics is not (at least in some limit) QFTCS. For example the event operator formalism has been proposed [36] as a way to make quantum mechanics consistent with certain pathologies that may, theoretically, arise in general relativity such as closed timelike curves or wormholes. A recent study has shown that an experiment distributing entangled photons between the ground and ISS could potentially distinguish this theory [9] from QFTCS. In future work we will explore the potential of the Franson experiment as a probe of the event operator theory.

Testing deviations from the standard relativity and quantum theories, requires highly sensitive measurements. In the case of entangled photon pairs propagating through a gravitational field, this supposes a high rate of pair generation and detection. In the simplest case the source and one of the detectors are located on the ground. This allows for the use of the best available technology. For the source, commercial lasers are available. The photons can be created by SPDC in commercial non-linear crystals or, for shorter wavelengths, in research grade crystals. The detectors are the component actually limiting the coincidence rate. Single photon detector arrays are the way to overcome the single detectors dead time. However, the multiplexing of a large number of detectors has its own limitations and requires specific development.

---

[1] Quantum technologies in space, `http://www.qtspace.eu/?q=organization`.

[2] Quantum technology flagship, `https://ec.europa.eu/digital-single-market/en/news/quantum-flagship-high-level-expert-group-publishes-final-report`.

[3] N. Gisin, R. Thew, Quantum communication, Nature Photonics 1.

[4] M. Krenn, M. Malik, T. Scheidl, R. Ursin, A. Zeilinger, Chapter: Quantum Communication with Photons, Book: Optics in Our Time, Springer International Publishing, 2016.

[5] H.-K. Lo, M. Curty, K. Tamaki, Secure Quantum Key Distribution, Nature Photonics 8 (August) (2015) 595–604.

[6] K. Edamatsu, Entangled photons: Generation, observation, and characterization, Japanese Journal of Applied Physics 46 (2007) 7175–7187.

[7] A. Fedrizzi, R. Ursin, T. Herbst, M. Nespoli, R. Prevedel, T. Scheidl, F. Tiefenbacher, T. Jennewein, A. Zeilinger, High-fidelity transmission of entanglement over a high-loss free-space channel, Nature Physics 5 (6) (2009) 389–392.

[8] P. A. Hiskett, D. Rosenberg, C. G. Peterson, R. J. Hughes, S. Nam, A. E. Lita, A. J. Miller, J. E. Nordholt, Long-distance quantum key distribution in optical fibre, New Journal of Physics 8 (9) (2006) 193.
URL http://stacks.iop.org/1367-2630/8/i=9/a=193

[9] S. K. Joshi, J. Pienaar, T. C. Ralph, L. Cacciapuoti, W. McCutcheon, J. Rarity, D. Giggenbach, V. Makarov, I. Fuentes, T. Scheidl, E. Beckert, M. Bourennane, D. E. Bruschi, A. Cabello, J. Capmany, J. A. Carrasco, A. Carrasco-Casado, E. Diamanti, M. Duusek, D. Elser, A. Gulinatti, R. H. Hadfield, T. Jennewein, R. Kaltenbaek, M. A. Krainak, H.-K. Lo, C. Marquardt, G. Milburn, M. Peev, A. Poppe, V. Pruneri, R. Renner, C. Salomon, J. Skaar, N. Solomos, M. Stipčević, J. P. Torres, M. Toyoshima, P. Villoresi, I. Walmsley, G. Weihs, H. Weinfurter, A. Zeilinger, M. Żukowski, R. Ursin, Space QUEST mission proposal: Experimentally testing decoherence due to gravity, arXiv, 1703.08036 (2017) 1–16.

[10] B. H. C. H. E. M.-S. C. E. B. H. Z. Y. H. H. G. W. E. C. I. D. D. H. R. L. T. Jennewein, J. P. Bourgoin, Qeyssat: a mission proposal for a quantum receiver in space, Proc.SPIE 8997 (2014) 8997 – 8997 – 7. doi:10.1117/12.2041693.

[11] J. Yin, Y. Cao, Y.-H. Li, S.-K. Liao, L. Zhang, J.-G. Ren, W.-Q. Cai, W.-Y. Liu, B. Li, H. Dai, G.-B. Li, Q.-M. Lu, Y.-H. Gong, Y. Xu, S.-L. Li, F.-Z. Li, Y.-Y. Yin, Z.-Q. Jiang, M. Li, J.-J. Jia, G. Ren, D. He, Y.-L. Zhou, X.-X. Zhang, N. Wang, X. Chang, Z.-C. Zhu, N.-L. Liu, Y.-A. Chen, C.-Y. Lu, R. Shu, C.-Z. Peng, J.-Y. Wang, J.-W. Pan, Satellite-based entanglement distribution over 1200 kilometers, Science 356 (6343) (2017) 1140–1144.

[12] G. Amelino-Camelia, C. Lämmerzahl, Quantum-gravity-motivated Lorentz-symmetry tests with laser interferometers, Classical and Quantum Gravity 21 (4) (2004) 899–915.

[13] A. Camacho, A. Macías, Deformed dispersion relations and the degree of the coherence function, General Relativity and Gravitation 38 (4) (2006) 547–551. doi:10.1007/s10714-006-0245-x.

[14] M. Zych, F. Costa, I. Pikovski, T. C. Ralph, Č. Brukner, General relativistic effects in quantum interference of photons, Classical and Quantum Gravity 29 (22) (2012) 224010.

[15] T. C. Ralph, G. J. Milburn, T. Downes, Quantum connectivity of space-time and gravitationally induced decorrelation of entanglement, Phys. Rev. A 79 (2009) 022121.

[16] N. D. Birell, P. C. W. Teich, Quantum fields in curved space, Cambridge University Press, 1982.

[17] J. W. Goodman, Introduction to Fourier Optics, Roberts and Company Publishers, 2005.

[18] B. E. A. Saleh, M. C. Teich, Fundamentals of Photonics, John Wiley & Sons, 2007.

[19] R. M. Wald, General Relativity, University of Chicago Press, Chicago, 1984.

[20] Y. Shih, An introduction to Quantum Optics, Taylor and Francis, Florida, 2011.

[21] D. E. Bruschi, T. C. Ralph, I. Fuentes, T. Jennewein, M. Razavi, Spacetime effects on satellite-based quantum communications, Phys. Rev. D 90 (2014) 045041.

[22] D. E. Bruschi, A. Datta, R. Ursin, T. C. Ralph, I. Fuentes, Quantum estimation of the schwarzschild spacetime parameters of the earth, Phys. Rev. D 90 (2014) 1–10.

[23] J. Kohlrus, D. E. Bruschi, J. Louko, I. Fuentes, Quantum estimation of physical parameters in the spacetime of a rotating planet, EPJ Quantum Technol. (2017) 4–7.

[24] R. J. Glauber, The Quantum Theory of Optical Coherence, Phys. Rev. 130 (6) (1963) 2529–2539.

[25] A. Zeilinger, Experiment and the foundations of quantum physics, Reviews of Modern Physics 71 (2) (1999) S288–S297.

[26] M. Genovese, Real applications of quantum imaging, Journal of Optics 18.

[27] D. N. Klyshko, Photon and Nonlinear Optics, Gordon and Breach Science Publishers, New York, 1988.

[28] M. V. Fedorov, Y. M. Mikhailova, P. a. Volkov, Gaussian modelling and Schmidt modes of SPDC biphoton states, Journal of Physics B: Atomic, Molecular and Optical Physics 42 (17) (2009) 175503.

[29] J. Franson, Bell inequality for position and time., Physical Review Letters 62 (19) (1989) 2205–2208.

[30] T. P. Wihler, B. Bessire, A. Stefanov, Computing the entropy of a large matrix, Journal of Physics A: Mathematical and Theoretical 47 (24) (2014) 245201.

[31] Y. Shih, Entangled photons, IEEE Journal of selected topics in quantum electronics 9 (6) (2003) 1455–1467.

[32] D. Richart, Y. Fischer, H. Weinfurter, Experimental implementation of higher dimensional timeenergy entanglement, Applied Physics B 106 (3) (2012) 543–550.

[33] R. Thew, a. Acín, H. Zbinden, N. Gisin, Bell-Type Test of Energy-Time Entangled Qutrits, Physical Review Letters 93 (1) (2004) 010503.

[34] B. Bessire, C. Bernhard, T. Feurer, A. Stefanov, Versatile shaper-assisted discretization of energy-time entangled photons, New Journal of Physics 16 (3) (2014) 033017.

[35] R. A. Clauser, John F.; Horne, Michael A.; Shimony, Abner; Holt, Proposed experiment to test separable hidden-variable theories, Phys. Rev. Lett. 23 (15) (1969) 880–884.

[36] T. C. Ralph, J. Pienaar, Entanglement decoherence in a gravitational well according to the event formalism, New Journal of Physics 16.

[37] C. Bonato, A. Tomaello, V. D. Deppo, G. Naletto, P. Villoresi, Feasibility of satellite quantum key distribution, New Journal of Physics 11. arXiv:0903.2160.

[38] S.-K. Liao, W.-Q. Cai, W.-Y. Liu, L. Zhang, Y. Li, J.-G. Ren, J. Yin, Q. Shen, Y. Cao, Z.-P. Li, F.-Z. Li, X.-W. Chen, L.-H. Sun, J.-J. Jia, J.-C. Wu, X.-J. Jiang, J.-F. Wang, Y.-M. Huang, Q. Wang, Y.-L. Zhou, L. Deng, T. Xi, L. Ma, T. Hu, Q. Zhang, Y.-A. Chen, N.-L. Liu, X.-B. Wang, Z.-C. Zhu, C.-Y. Lu, R. Shu, C.-Z. Peng, J.-Y. Wang, J.-W. Pan, Satellite-to-ground quantum key distribution, Nature.

[39] T. B. Pittman, D. V. Strekalov, D. N. Klyshko, M. H. Rubin, A. V. Sergienko, Y. H. Shih, Two-photon geometric optics, Phys. Rev. A 53 (4) (1996) 2804–2815.

[40] W. P. Grice, I. A. Walmsley, Spectral information and distinguishability in type-II down-conversion with a broadband pump, Physical Review A - Atomic, Molecular, and Optical Physics 56 (2) (1997) 1627–1634.

[41] C. Kurtsiefer, M. Oberparleiter, H. Weinfurter, Generation of correlated photon pairs in type-II parametric down conversionrevisited, Journal of Modern Optics 48 (13) (2001) 1997–2007.

[42] S. Takeuchi, Beamlike twin-photon generation by use of type II parametric downconversion., Optics letters 26 (11) (2001) 843–5.

[43] Y. H. Kim, W. P. Grice, Generation of pulsed polarization-entangled two-photon state via temporal and spectral engineering, Journal of Modern Optics 49 (14-15) (2002) 2309–2323.

[44] Y.-H. Kim, W. P. Grice, Measurement of the spectral properties of the two-photon state generated via type II spontaneous parametric downconversion, Optics Letters 30 (8) (2005) 908.

[45] G. Brida, M. V. Chekhova, I. P. Degiovanni, M. Genovese, G. K. Kitaeva, A. Meda, O. A. Shumilkina, Biphoton compression in a standard optical fiber: Exact numerical calculation, Physical Review A - Atomic, Molecular, and Optical Physics 81 (5) (2010) 1–8.

[46] G. Brida, M. V. Chekhova, I. P. Degiovanni, M. Genovese, G. K. Kitaeva, A. Meda, O. A. Shumilkina, Chirped Biphotons and their Compression in Optical Fibers, Physical Review Letters 103 (19) (2009) 1–4.

[47] M. B. Nasr, S. Carrasco, B. E. A. Saleh, A. V. Sergienko, M. C. Teich, J. P. Torres, L. Torner, D. S. Hum, M. M. Fejer, Ultrabroadband Biphotons Generated via Chirped Quasi-Phase-Matched Optical Parametric Down-Conversion, Phys. Rev. Lett. 100 (18) (2008) 183601.

[48] B. Dayan, A. Pe'er, A. Friesem, Y. Silberberg, Nonlinear Interactions with an Ultrahigh Flux of Broadband Entangled Photons, Physical Review Letters 94 (4) (2005) 043602.

[49] G. Brida, I. P. Degiovanni, F. Piacentini, V. Schettini, S. V. Polyakov, A. Migdall, Scalable multiplexed detector system for high-rate telecom-band single-photon detection, Review of Scientific Instruments 80 (11).

[50] S. A. Castelletto, I. P. Degiovanni, V. Schettini, A. L. Migdall, Reduced dead time and higher rate photon counting detection using a multiplexed detector array, J Mod Opt 54 (May) (2007) 337–352.

[51] L. H. Braga, L. Gasparini, L. Grant, R. K. Henderson, N. Massari, M. Perenzoni, D. Stoppa, R. Walker, A fully digital 816 sipm array for pet applications with per-pixel tdcs and real-time energy output, IEEE Journal of Solid-State Circuits 49 (1) (2014) 301–314.

[52] L. Gasparini, et al., A 32×32-pixels time-resolved single-photon image sensor with 44.64μm pitch and 19.48% fill factor with on-chip row/frame skipping features reaching 800 kHz observation rate for quantum physics applications, IEEE Journal of Solid-State Circuits, 2017 accepted, in press.

[53] S. Sukegawa, T. Umebayashi, T. Nakajima, H. Kawanobe, K. Koseki, I. Hirota, T. Haruta, M. Kasai, K. Fukumoto, T. Wakano, K. Inoue, H. Takahashi, T. Nagano, Y. Nitta, T. Hirayama, N. Fukushima, A 1/4-inch 8Mpixel back-illuminated stacked CMOS image sensor, Digest of Technical Papers - IEEE International Solid-State Circuits Conference 56 (1) (2013) 484–485.

[54] C. W. Stubbs, F. W. High, M. R. George, K. L. DeRose, S. Blondin, J. L. Tonry, K. C. Chambers, B. R. Granett, D. L. Burke, R. C. Smith, Toward More Precise Survey Photometry for PanSTARRS and LSST: Measuring Directly the Optical Transmission Spectrum of the Atmosphere, The Publications of the Astronomical Society of the Pacific 119 (2007) 1163.

[55] A. C. Busacca, E. D'Asaro, A. Pasquazi, S. Stivala, G. Assanto, Ultraviolet generation in periodically poled lithium tantalate waveguides, Applied Physics Letters 93 (12) (2008) 1–4.

[56] P. Delva, A. Hees, S. Bertone, E. Richard, P. Wolf, Test of the gravitational redshift with stable clocks in eccentric

orbits: application to galileo satellites 5 and 6, Classical and Quantum Gravity 32 (23) (2015) 232003.
URL http://stacks.iop.org/0264-9381/32/i=23/a=232003

[57] G. Giorgi, M. Lülf, C. Günther, S. Herrmann, D. Kunst, F. Finke, C. Lämmerzahl, Testing general relativity using Galileo satellite signals, European Signal Processing Conference 2016-November (2016) 1058–1062.